Towards braided shape memory polymer surgical sutures

by

Bora Ferruh Uz

A thesis submitted in partial fulfillment of the requirements for the degree of

Master of Science

Department of Mechanical Engineering

University of Alberta

Abstract

Surgical sutures are used for wound closure in surgeries and injuries by bringing the edges of an open wound together. Conventional way of applying surgical sutures is to secure the wound with surgical knots and tight stitches. Compared to conventional ones, braided sutures have advantages in terms of pliability, handling, and knot security. Some of the typical suture materials are chromic/plain catgut, silk, and syntheticpolymers such as polyglactin and polyamide. In this study, a type of smart material, namely shape memory polymer (SMP), is proposed as an alternative surgical suture material to produce braided sutures that can be stitched loosely and are able to self-tighten when their shape memory effect (SME) is activated. Mechanical and SME properties of SMPs can be improved by reinforcing them with cellulose nanocrystals (CNCs) which is a biocompatible nanosized material that offers high mechanical properties. In the present study, braided SMPs and CNC reinforced SMPs are produced. The effect of braiding parameters along with effect of the amount of CNC wt% in SMPs are investigated through a series of experiments to analyze mechanical and SME properties. The results indicated that mechanical properties reduced with increasing braid angle. A prediction model for the elastic modulus of braided SMPs were adopted and accurate results were obtained between the predicted and experimentally obtained values. Shape recovery rate decreased with increasing number of core filaments, whereas maximum shape recovery was not affected by any of the braiding parameters. Recovery stresses were similar with the exception of braids with three core filaments where they showed poorer performance. Addition of CNC reduced the mechanical performance of the braids, while SME properties were improved. Recovery stresses increased by 100.5% when the braids made of

neat SMP and SMP with 4.0 wt% CNC were compared. Although elastic moduli of all type of braids were comparable to that of commercially available sutures, relatively poor tensile strength should be addressed.

Acknowledgements

I would like to express my deepest appreciation and gratitude to my supervisor, Dr. Cagri Ayranci, who has patiently helped and guided me throughout my graduate training and research in University of Alberta.

A very special thanks goes to our group member Irina Garces for always showing the way and helping me with the laboratory equipment, materials, and techniques I have used throughout this research.

I would like to thank my girlfriend Figen Karaca. She has always been there for me with her unconditional help and never-ending support; both emotionally and work-wise. This journey would be much less enjoyable and harder of a challenge without her.

Finally, I am deeply grateful to my parents for their trust and encouragement. They are always there for me with their guidance and support. Thank you for standing by me.

Contents

List of Figures

List of Tables

Chapter 1: Introduction

Sutures are commonly used during surgeries for wound closure. The conventional use of a suture is to bring two edges of an open wound together to apply tight stitches and surgical knots with the use of threads. Stitches must apply a certain amount of tension to the sides of the wound for a proper healing process [1, 2]; therefore, tensile properties of the suture material are crucial. An optimal suture would have similar stress-strain behavior with the tissue that it is applied on [3, 4]. Sutures can be classified based on number of strands; those that consist of single and multiple filament(s) [3, 5]. Multifilament sutures can be produced by a technique called braiding in which three or more yarns or filaments are intertwined together. Compared to monofilament sutures, braided multifilament sutures offer advantages in terms of pliability, handling, and knot security [6]. Additionally, they provide tailorability of mechanical properties due to the inherent ability of the braiding technology (e.g. control over braid angle).

Some of the conventional suture materials are chromic/plain catgut, silk, and synthetic polymers such as polyglactin and polyamide [6, 7]. As an alternative to conventional ones, smart materials, namely shape memory polymers (SMPs) are also studied [2, 8]. SMPs are able to retain their original shape after a large deformation through their shape memory effect (SME) which is activated by an external stimulus such as temperature, stress, pressure, and electric current etc. [9]. If this external stimulus is temperature, i.e. SMP is thermoresponsive, SMP starts to return to its original shape when it is heated through its glass transition temperature [10].

There are numerous research on the applications of SMPs including self-tightening and self-unraveling monofilament sutures [2, 8]. By manufacturing filaments using SMPs with glass transition temperature above the normal human body temperature, it is possible to produce sutures that can be stitched loosely and are able to self-tighten when their SME is activated, which would eliminate the difficulty of tying surgical knots in a limited space [2, 8, 11]. A drawback of SMPs is their low mechanical properties and shape recovery forces. This can be addressed by reinforcing them with cellulose nanocrystals (CNC) that offer high mechanical properties for the braided sutures to form CNC reinforced SMP braids.

In this thesis, SMP and CNC reinforced SMP are proposed as an alternative materials to produce braided surgical sutures due to the shape memory feature of the SMPs and pliability of the braiding technique. Their mechanical properties in glass state (elastic modulus, ultimate tensile strength) and shape recovery properties (shape fixity, shape recovery rate, maximum recovery, shape recovery force) are investigated for various types of braid configurations and different wt% of CNC reinforcement. The study focuses on providing a proof of concept for SMP and CNC reinforced SMP braided sutures along with investigating braided SMP and CNC reinforced SMP structures in general.

1.1 Background

In this section, background information on the materials, concepts and manufacturing techniques that were used throughout the preparation of this thesis is presented. Shape memory materials and its subcategory, SMPs, are introduced along with their main feature, SME, and potential applications in Subsection 1.1.1. In Subsection 1.1.2, information on braiding

technique, braid patterns, and working principles of maypole braider are provided. CNCs and their possible application as a filler material inside polymer matrices are mentioned in Subsection 1.1.3.

1.1.1 Shape memory polymers

Shape memory materials (SMMs) are materials that can return to their original shapes through a stimulus when deformed to a temporary shape. The ability of these materials to remember and return to their original shapes is called SME. Although a number of different SMMs exist such as shape memory gels, shape memory ceramics, and shape memory hybrids, traditional SMMs that have been extensively studied so far are shape memory alloys (SMAs) and SMPs. SMPs have major advantages over other SMMs, especially SMAs. Some of these advantages are ease of tailoring material properties, low cost, ease of manufacturing, and in most cases biocompatibility and/or biodegradability. They are also very light weight and the amount of shape recovery is significantly higher compared to SMAs. SME of SMPs can be actuated through many different types of stimuli such as heat, moisture, pH change or light [9, 11, 12].

SMPs are studied extensively for many promising potential applications. Some of the examples are reusable Braille papers, self-tightening and loosening screws, hinge in morphing wings for aerospace applications, self-grasping spoons and forks, sportswear [9]. Biomedical applications are another area of interest for use of SMPs due to their advantages such as biocompatibility. Maitland et al. (2002) reported a clot removal device made of thermo-responsive SMP that is able to transform from a narrow shape to a form that is able grab the clot inside

the artery [13]. Moreover, many researchers have focused on SMP vascular stents that would self-expand in the artery which can also achieve drug release [9, 11, 14, 15, 16, 17, 18, 19]. Other biomedical applications include SMP cardiac valve repair rings, soft tissue fixation devices made of SMP for fixing anterior cruciate ligament tears, SMP arch wire braces for teeth [11, 20, 21]. Furthermore, a monofilament surgical suture made of SMP with self-tightening ability was developed by Lendlein (2002). The suture was able to self-tighten and close the wound after actuation when applied loosely to a rat [2].

Polyurethane based thermoplastic SMPs are widely popular among researchers because they show good SME characteristics and are commericalized [9]. Most SMPUs are thermoplastic meaning that original shape of the processed material can be changed multiple times when heated above a certain temperature unlike thermosets, which eases the production of the former. Shape memory polyurethanes (SMPUs) are composed of crystalline (hard, elastic) and amorphous (soft, transition) segments, and hence they are semi-crystalline structures. Crystalline segments are hard and brittle at temperatures lower than their melting temperature, whereas amorphous segments have these characteristics at temperatures less than their glass transition temperature [9, 10]. Glass transition temperature represent the point where amorphous segments transition from glassy to rubbery state. It should be noted that transition to glass state occurs over a range of temperatures (glass transition region), in which the mid-point of this transition region is known as glass transition temperature [9]. When heated above glass transition temperature, amorphous segments switch to rubbery state, and become soft and flexible, while crystalline segments remain in glassy state if melting temperature of the crystalline segments are higher than glass transition temperature of

amorphous segments. Due to switch to rubbery phase, elastic modulus of the amorphous regions decreases and allows SMPU to be deformed to a temporary shape. This temporary shape is fixed upon cooling since amorphous segments switch to glassy state and harden again. Elastic energy increases in crystalline segments during this deformation and it is stored as the temporary shape is fixed. If the material is heated through the glass transition temperature of the amorphous segments once again, overall structure attempts to retain its original shape due to stored elastic energy in crystalline segments because amorphous segments soften and are no longer able to hold the temporary shape [10]. Consequently, crystalline regions are responsible for retaining the original shape, while amorphous regions are responsible for fixing the temporary shape.

The ability to recover the original shape, whose mechanism is explained above, is called SME and it can be quantified by certain characteristics, namely, shape fixity, shape recovery rate, maximum recovered strain, and shape recovery force. Shape fixity is the amount of fixed strain after deformation above glass transition temperature. Shape recovery rate and maximum recovered strain are expressed as the speed of the recovery and the maximum amount of recovered strain, respectively. The amount of force applied during recovery due to stored elastic energy is called shape recovery force. These characteristics are influenced by the contents of the crystalline and amorphous segments.

1.1.2 Braided structures

Braiding is a versatile production technique where three or more strands of filaments, yarns, or wires are intertwined around an axis to produce a stronger product. They are used in

a wide range of applications such as ropes, cables, and hoses. Braiding technique is also utilized in composite structures where braids act as the reinforcement [22]. Fan blades, stators, and propellers in aircraft engines, hockey sticks, shafts in high performance cars are some of the applications of braided composite structures. In addition, braided surgical sutures and braided coronary stents are commonly used in medical field [22, 23].

Braids can be classified by their geometries (two-dimensional, three-dimensional, multidirectional) or final shapes (flat, tubular, three-dimensional) [22, 24]. Two-dimensional tubular or linear rope-like braids can be manufactured in maypole braiders in various patterns based on strand overlapping configurations. One of the most common patterns is the diamond pattern where each strand overlaps the next one. Figure 1.1 shows the interlacing pattern of the strands of a diamond braid geometry. Colors of the strands represent the directions they move in, namely, clockwise (CW) and counterclockwise (CCW). If $X1$ is the longitudinal axis of the braid, θ is defined as the braid angle; the angle that strands make with the longitudinal axis. Braid angle is critical in determination of the mechanical characteristics of braids and is governed by a number of parameters (e.g. shape and thickness of the strands, braid diameter, take-up speed of the braider, and rotational speed of the horn gears).

Maypole braiders -the kind that was adopted in this thesis- are commonly used to produce two dimensional tubular or linear braids. They consist of two main mechanisms, namely, track plate and take-up. Sketch of a braider is shown in Figure 1.2. Track plate is responsible for the maypole dance-like movement of the carriers, whereas take-up mechanism pulls the strands as they are interlaced together.

Track plate involves gears, motors, horn gears, and carriers [23]. Gears are attached un-

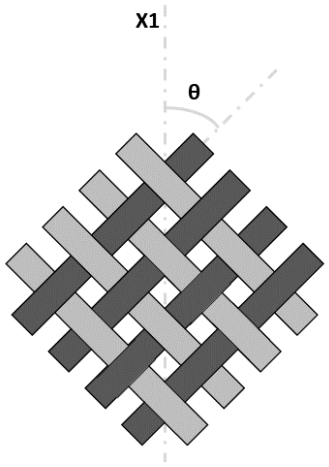

Figure 1.1: Strands in diamond braid pattern.

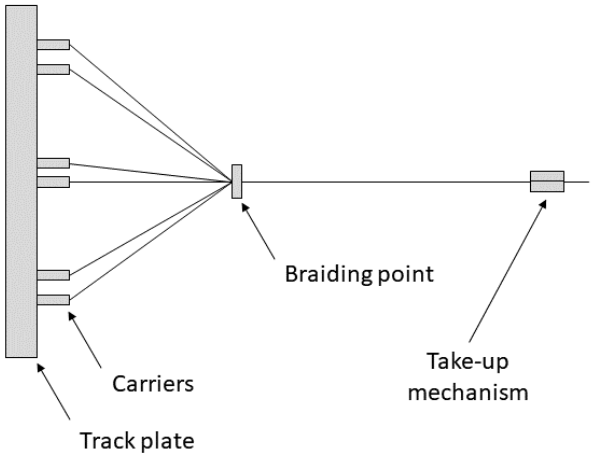

Figure 1.2: Sketch of the components a braider.

derneath horn gears and are driven by the motor(s). Horn gears rotate around their center axis in order to move the carriers to their neighboring horn gear. Figure 1.3 illustrates the movement of three carriers rotating in each direction for a 18 horn gear maypole braider. Braid pattern in Figure 1.3 is diamond (1 over, 1 under) which is determined by the positions of the carriers. Different braid patterns such as regular (2 over, 2 under) and hercules (3 over, 3 under) can be obtained by installing carriers in various combinations. In Figure 1.3, strands A, C, E are moving in CCW direction, whereas B, D, F are moving in CW direction. Pairs A-B, C-D, and E-F approach each other in Figure 1.3a and 1.3b. Figure 1.3c is where the strands that rotate in CCW direction go above their CW rotating pairs. In Figures 1.3d, 1.3e, 1.3f pairs move away from each other. After Figure 1.3f, the next encounter will be between the pairs A-F, B-C, and D-E in which the ones that rotate in CW direction will go over their CCW rotating pairs. As the carriers move and strands are locked together at the braiding point (Figure 1.2), take-up mechanism pulls the produced braid. Steady state motion of the track plate and take-up mechanism generates braids and determines the braid angle. Methodology and geometry of the braids that were produced for this study are further discussed in Section 2.3 and visual representations are presented in Figure 2.5.

1.1.3 Cellulose nanocrystals

Cellulose is an organic polymer and quiet abundant in nature [10]. Many living organisms such as plants and animals contain cellulose in both crystalline and amorphous orders [25]. Size of crystalline cellulose is in the order of nanometers [26]. Some of the main advantages of cellulose are its high stiffness and light-weight. In addition, since cellulose is a biopolymer, it

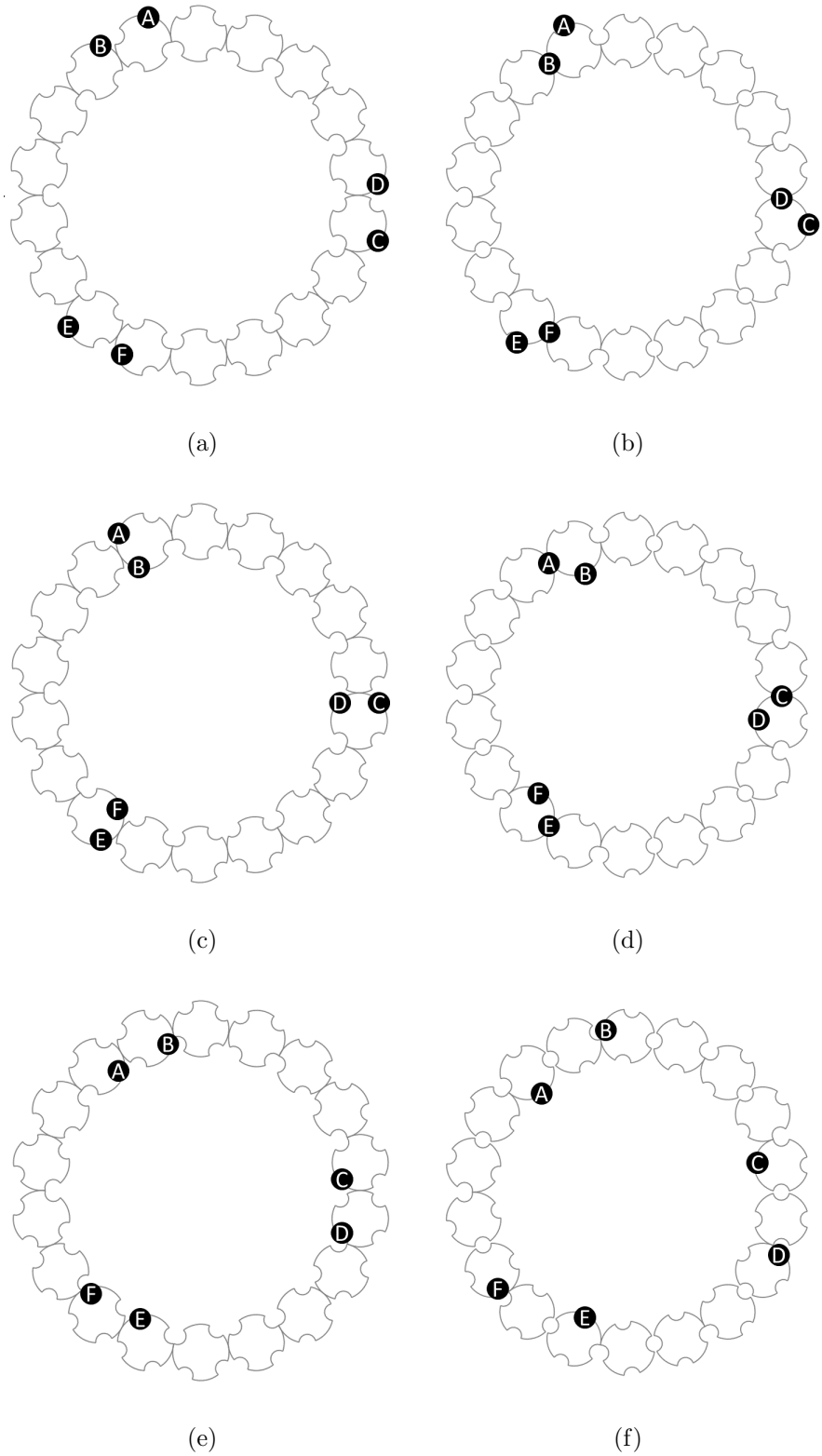

Figure 1.3: Movement of the carriers on a 18 horn gear maypole braider. Carrier pattern is for diamond braid with 6 strands; rotating in CW and CCW directions.

is biocompatible and biodegradable which makes it suitable for biomedical applications [10]. In order to produce CNC, individual nanofibers can be isolated by chemical or enzymatic treatment followed by acid hydrolysis or mechanical treatment from the naturally existing form of cellulose [26].

Highly crystalline order, large surface area, and good interaction characteristics with other polymers make CNC a suitable material to be used as reinforcement in polymer composites [27, 28]. Hence, shortcomings of SMPs like low strength, stiffness, or recovery force can be overcome by reinforcing SMPs with a filler material such as CNC. Moreover, thermal properties governing the SME can also be improved with the addition of CNC [26]. The effect of CNCs on SMPs depends on wt% of CNC, interfacial adhesion between CNC and SMP, aspect ratio of the CNCs, and method of mixing these two [26]. Methods for producing CNC reinforced SMP include extrusion, hot pressing, and evaporation, among which the first shows the least reinforcement efficiency [29].

1.2 Overview of the thesis

This thesis is divided into two main parts, namely, investigation of braided SMPs and braided CNC reinforced SMPs along with their applicability in biomedical field, specifically for surgical sutures. The goal of the first part was to analyze the effect of braiding parameters on mechanical and SME properties of the braided SMP in order to investigate its suitability as a suture material. The second part aimed to investigate the effects of the amount of CNC on the mechanical and SME properties of braided CNC reinforced SMP. Similar methodologies were followed for both parts. First, materials were melt extruded into filaments, then

filaments were braided. Tensile and SME tests were conducted for filaments and braids. All these procedures were explained in detail in Chapter 2. Results of the tests, discussions on the results, and comparisons to commercially available sutures were made in Chapter 3 and 4. The former describes the effect of braiding parameters on braided SMP, whereas effect of CNC on the CNC reinforced SMP braids was investigated in the latter.

Chapter 2: Materials & methodology

2.1 Materials

The raw SMP material was a commercially available thermoplastic SMPU known as MM4520 and was purchased from SMP Technologies, Japan in pellet form. Glass transition temperature of this material is reported to be approximately 45 °C [30, 31, 32]. MM4520 is biocompatible, hence, suitable for biomedical applications including suture material [9, 33, 34].

CNC was used as a filler material to reinforce polymer matrix and it was provided by InnoTech Alberta. The diameter and length of the nanoparticles ranged between 5-10 nm and 100-200 nm, respectively, as reported by InnoTech Alberta. In addition to biocompatibility, CNC is also biodegradable as opposed to MM4520 [35].

2.2 Material extrusion

In order to prepare SMPU filaments, MM4520 pellets were dried for 24 hours in Lindberg/Blue™ vacuum oven at 80 °C prior to extrusion in order to avoid formation of voids inside the filaments [31]. They were placed in vacuum bags after removal from the vacuum oven. The pellets were fed to a single screw Brabender Laboratory Extruder® coupled with ATR Plasti-Corder® Torque Rheometer. The extrusion rate was set to 5 RPM and temperatures of the chambers to 160 °C, 170 °C, 180 °C, 195 °C (ordered from feeder to nozzle of the extruder). A take-up/winding mechanism was used to collect the filaments around a 152 mm diameter spool rotating at 41.5 RPM. A conveyor belt and a high temperature

silicon ring were placed across the collector in order to obtain consistent diameters along the spool during filament collection, which was a process similar to the production technique called filament winding. The high rotation speed of the collector reduced the diameter of the filament after it left the extruder's nozzle. No cooling mechanism was present.

To obtain CNC reinforced SMPU nanocomposites, MM4520 pellets and CNC particles were melt extruded in Prism Usalab 16 twin screw extruder at InnoTech Alberta, Edmonton, AB. In order to prepare the master batch, their weight ratios were adjusted to 96% and 4%, respectively, and were mixed prior to melt extrusion. All sections throughout the barrel of the extruder were set to 200 °C and the rotational speed to 100 RPM. The produced filaments were shredded into pellets for ease of mixing further SMPU pellets to obtain various CNC wt%. Additional MM4520 pellets were added to the master batch in order to produce CNC reinforced SMPU with 0.5, 2, and 4 CNC wt%. Rest of the melt extrusion process was identical to that of neat SMPU filaments, which was explained previously.

Same filler and polymer matrix were mixed together using a similar procedure previously by Garces et al. (2018) [36]. T_g values of the resulting nanocomposites were investigated through differential scanning calorimetry and it was found that CNC addition did not change T_g of the polymer matrix. Same observation was made in another study which also investigated CNC reinforced SMPUs [10].

Resulting filament diameters were measured with a micrometer at 50 different locations. Mean diameters and standard deviations are shown in Table 2.1. Box plot containing medians, interquartile ranges, and extremes of diameter measurements is given in Figure 2.1.

All filaments were wrapped around bobbins of the braiding machine, and contained in zipper

Table 2.1: Filament diameters.

CNC wt%	Diameter (mm)	
	Mean	Standard deviation
0.0	0.420	0.018
0.5	0.438	0.026
2.0	0.425	0.024
4.0	0.419	0.025

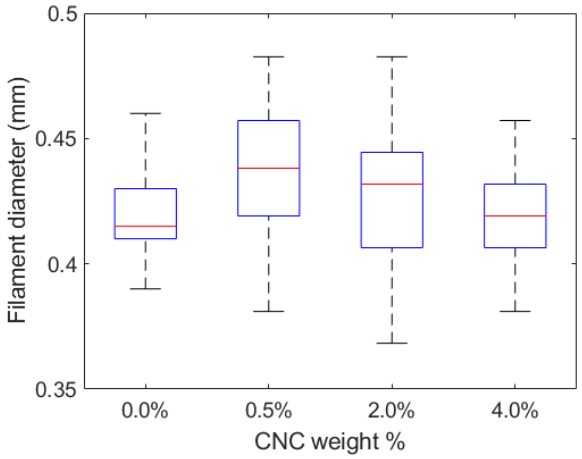

Figure 2.1: Box plot for filament diameters of different CNC wt%.

storage bags with silica gel beads until braiding.

2.3 Braiding

The braids for this study were produced using Steeger USA K80-72 Maypole braider. Bobbins and carriers of the braider can be seen in Figure 2.2. Although the braider can take up to 36 carriers, only 6 carriers were installed to obtain a diamond braid pattern with 3 filaments rotating in each direction (CW and CCW). The rotational speed of the horn gears was kept constant at 75 RPM. For Chapter 3, the design parameters for the braids were take-

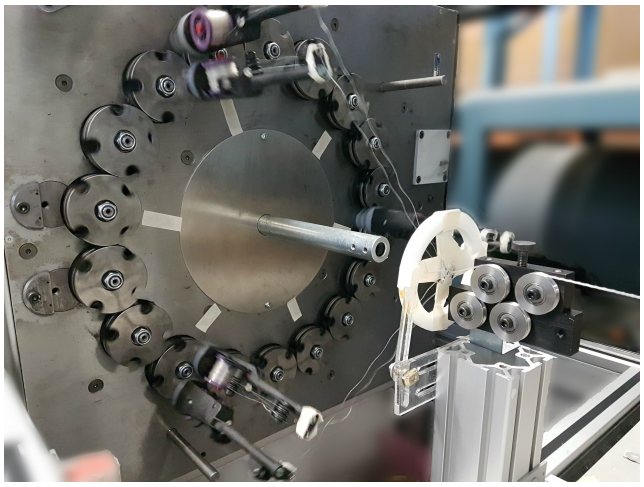

Figure 2.2: A picture of the Steeger USA K80-72 Maypole braider.

up speed and number of core filaments. Three different take-up speeds were introduced to obtain various braid angles (the angle between the filaments and the longitudinal axis of the braid). This was done by setting picks-per-inch (PPI) option of the braiding machine to 8, 12, and 16, which was inversely proportional to actual take-up mechanism speed. Consequent take-up speeds were measured to be 3.99 mm/sec, 2.67 mm/sec, 2.00 mm/sec for PPI values 8, 12, 16, respectively. The filaments were braided around 1 and 3 filament(s) which form(s) the core, with all three take-up speed settings. A set without any core filaments was also produced, resulting in a total of 9 different braid types.

Geometric models were prepared in order to predict braid angles. Geometry of the braids without any core filaments is shown in Figure 2.3. Solid and dashed lines represent two types of possible geometries at the instants that filaments are undulating on one another. Since there are three filaments rotating in each direction, they intertwine with the filaments that are rotating in opposite direction at every 1/6 cycle, i.e. every 60°s. Example movements of

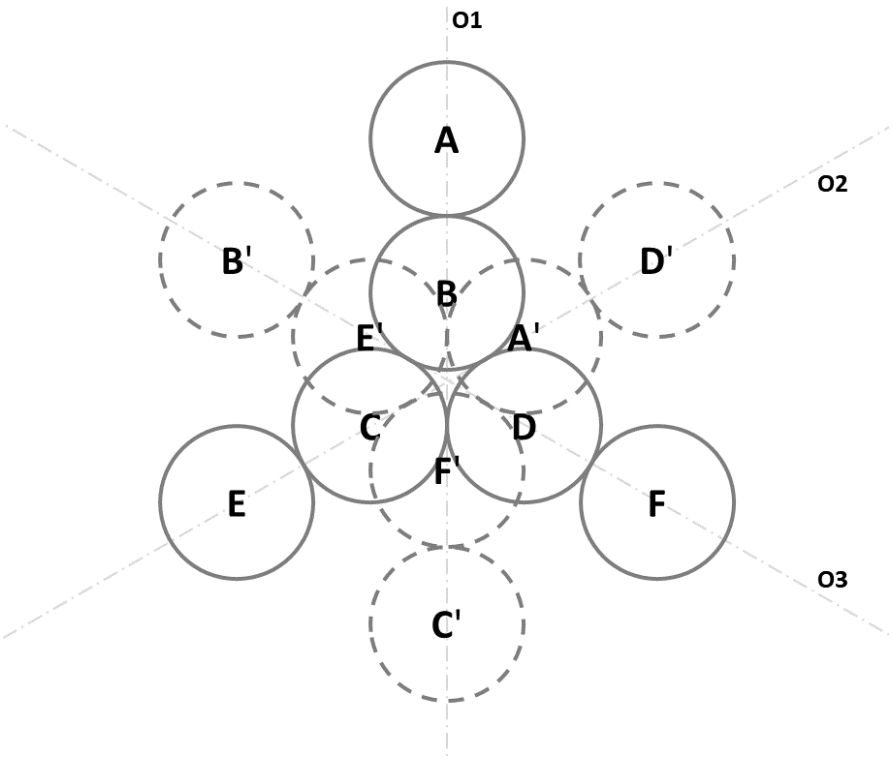

Figure 2.3: Geometry of the braids without any core filaments.

filaments rotating in each direction are described below for a full cycle using Figure 2.3.

$$\text{(Clockwise)}\, A \rightarrow A' \rightarrow F \rightarrow F' \rightarrow E \rightarrow E' \rightarrow A$$

$$\text{(Counterclockwise)}\, B \rightarrow B' \rightarrow C \rightarrow C' \rightarrow D \rightarrow D' \rightarrow B$$

While filaments rotate as described around the longitudinal axis, they also move in the longitudinal direction due to take-up mechanism. Geometric visualization of this three dimensional movement is shown in Figure 2.4. A and A' in Figures 2.3 and 2.4 represent the same points. $(X1\,X2)$ plane in Figure 2.4 is the plane shown in Figure 2.3, whereas $X3$ is aligned with the longitudinal axis of the braid. The filament moves from point A to A'. Therefore, (OA') and (OA) are the distances travelled in $(X1X2)$ plane and longitudinal direction, respectively. The angle filament makes with the longitudinal axis of the braid is

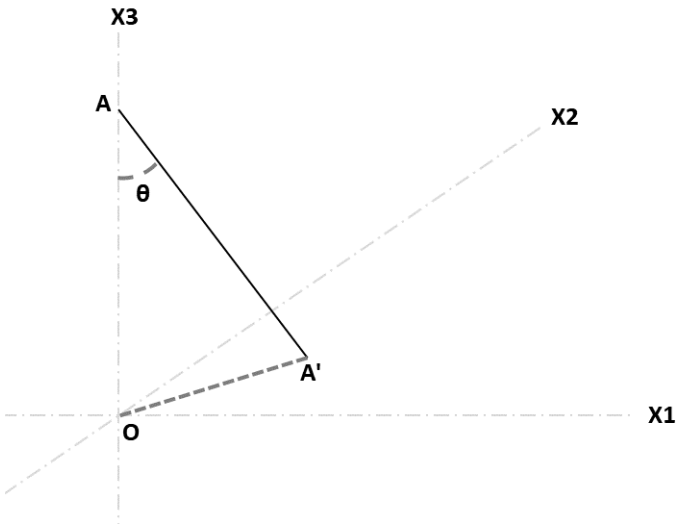

Figure 2.4: Movement of a filament in three dimensions.

θ, i.e. braid angle. Thus, braid angle can be found by calculating the lengths of (OA) and (OA'). The length of (OA') was calculated from the geometry in Figure 2.3 and given in equation (2.1).

$$(OA') = d\sqrt{\frac{4+\sqrt{3}}{3}} \tag{2.1}$$

Length (OA) is related to the speed of the take-up mechanism, V, and rotational speed of the carriers, ω. Since there are 18 horn gears in the braider, the distance travelled by a carrier to complete a full cycle is $9\pi\, d_{HG}$ due to geometry of the maypole braider where d_{HG} is the diameter of a horn gear. By dividing this value to the speed of the horn gears, time needed for a full cycle, t, can be found.

$$t = \frac{9\pi\, d_{HG}}{\omega\, d_{HG}/2} = \frac{18\pi}{\omega} \tag{2.2}$$

Since t in equation (2.2) is for a full cycle, it should be divided by 6 to find the time it takes for 1/6 cycle. By multiplying the resulting expression with V, distance (OA) can be found.

Final expression for (OA) is given in equation (2.3).

$$(OA) = \frac{3\pi V}{\omega} \tag{2.3}$$

Equations (2.1) and (2.3) are combined to find braid angle which is presented in equation 2.4 for braids with no core filaments.

$$\theta = \tan^{-1}\frac{(OA')}{(OA)} = \tan^{-1}\left(\frac{\omega d}{3\pi V}\sqrt{\frac{4+\sqrt{3}}{3}}\right) \tag{2.4}$$

Rotational speed of the horn gears, ω, was set to 75 RPM (= 2.5π rad/sec). Filament diameters, d, were provided in Table 2.1. Take-up speeds, V, for different braids were 3.99, 2.67, and 2.00 mm/sec.

For the braids with one and three core filament(s), equation (2.3) is applicable, however, equation (2.1) changes due to different braid geometry. Their two dimensional geometries are provided in Appendix A for the instances where filaments intertwine on one another. Equations (2.5) and (2.6) give the braid angles for braids with one and three core filament(s), respectively, similar to equation (2.4).

$$\theta = \tan^{-1}\left(\frac{\omega d}{\sqrt{3}\pi V}\right) \tag{2.5}$$

$$\theta = \tan^{-1}\left(\frac{\omega d}{3\pi V}\sqrt{\frac{10+3\sqrt{3}}{3}}\right) \tag{2.6}$$

Expected braid angles obtained from the geometric models are presented in Table 2.2 along with the braid angles measured from the actual samples. To obtain the braid angles from actual samples, one of the undulating filaments was painted blue using a marker pen for each braid type. Then, the angle between the colored undulating filament and longitudinal axis

Table 2.2: Braiding parameters and resulting braid angles.

# of core filaments	Take-up speed (mm/sec)	Braid angle (geometry)	Braid angle (measured)	
			Average	Standard deviation
3	3.99	11.2°	11.9°	1.2°
3	2.67	16.5°	14.9°	0.9°
3	2.00	21.5°	22.5°	1.4°
1	3.99	8.7°	8.5°	1.3°
1	2.67	12.8°	12.3°	1.8°
1	2.00	16.9°	17.6°	2.0°
0	3.99	6.9°	7.3°	0.7°
0	2.67	10.3°	9.5°	1.2°
0	2.00	13.6°	12.8°	1.9°

of the braid was measured at five different locations. Errors for measured braid angles with respect to braid angles obtained from the geometry ranged between 2.2% to 9.5%, which indicates that assumed geometries were relatively accurate. Example braid geometries were visualized using a CAD software and are shown in Figure 2.5.

Same methodology was followed in Chapter 4, however, only one braid configuration from Chapter 3 was adopted for each CNC wt%. The take-up speed for the selected configuration was 2.67 mm/sec with no core filaments.

2.4 Tensile testing methodology

Uniaxial tension tests were conducted at room temperature ($\approx 25\,^{\circ}\mathrm{C}$) which is notably below glass transition temperature of the materials under investigation. Produced braids were cut into 70 mm pieces to prepare specimens for tensile testing. To prevent clamp breaks during experiments, 10 mm from both ends of the specimen were tabbed with Cold Cure epoxy

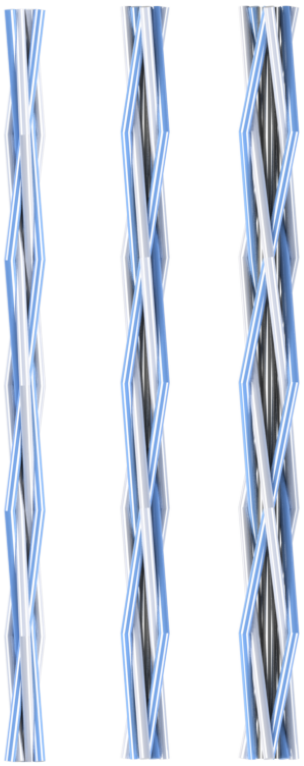

(a) (b) (c)

Figure 2.5: Example braid geometries (a) without any core filaments (b) with 1 core filament (c) with 3 core filaments.

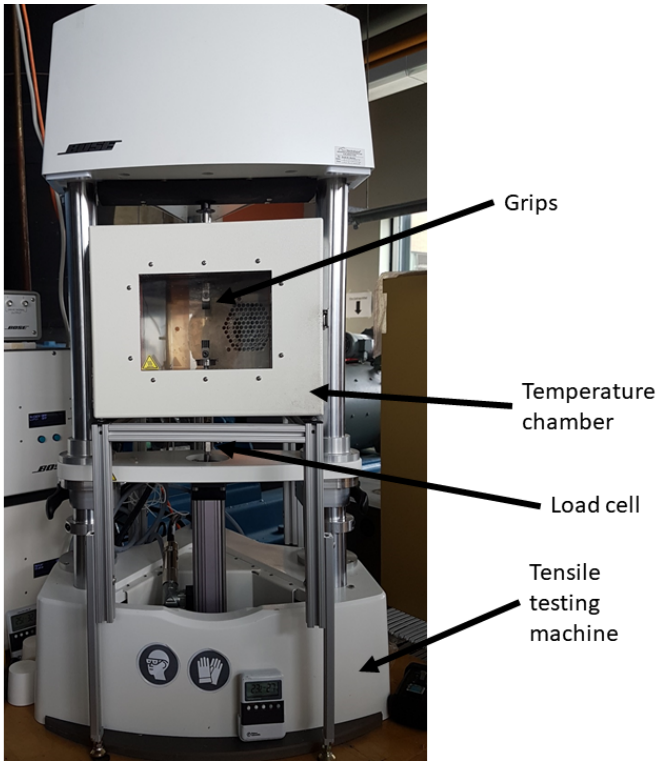

Figure 2.6: TA Instruments ElectroForce® 3200 Series III

resin [37]. In order to obtain consistent gauge lengths among samples, the epoxy had to be applied while specimen was positioned vertically to prevent leakage. Hence, end tabbing was conducted one at a time such that one end was tabbed and specimens were left for 24 hours to allow for curing. Then the same procedure was applied for the other end.

The tests were run using TA Instruments ElectroForce® 3200 Series III equipped with a 450 N (100 lb-f) Bose load cell (Figure 2.6). Specimens were clamped by tightening the grips to 15 in-lb using a torque wrench. Tabbed parts were kept inside the clamps leaving a nominal gauge length of 50 mm. A pretension of 0.3 N was applied to remove possible crimps. Displacement of the clamps was recorded when 0.3 N pretension was reached and this value was added/subtracted to/from the nominal gauge length, 50 mm, to find the

effective gauge length. Specimens were elongated to 45 mm in displacement ($\approx 90\%$ strain) at a constant rate of 0.5 mm/sec. Displacement and load data were acquired at 10 Hz during tests. Longitudinal elastic modulus and ultimate tensile strength (UTS) of the braids were calculated using the acquired data. Rupture could not be observed due to machine limitations, i.e. 45 mm of elongation was not sufficient for failure. Displacement data and effective gauge lengths were used to find strain based on equation (2.7).

$$\epsilon = \Delta L/L \tag{2.7}$$

where ΔL and L are displacement and effective gauge length, respectively.

The area had to be known for stress calculations, however, measurement was not possible since the braids consisted of multiple filaments and there were no coating or matrix present. Therefore, the area for each braid was calculated using respective braid geometry and average filament diameter as per equation (2.8). Resulting area values are shown in Table 2.3. The values in Table 2.3 are only valid when the filament diameter is 0.420 mm, i.e. for the braids produced with pure SMPU filaments.

$$A = N_{core}\frac{\pi d^2}{4} + N_{angle}\frac{\pi d^2}{4cos\theta} \tag{2.8}$$

where N_{core} and N_{angle} are number of core and undulating filaments, respectively, d is filament diameter and θ is braid angle.

Stress values were found as shown in equation (2.9) using recorded force values and the area calculations described in equation (2.8).

$$\sigma = F/A \tag{2.9}$$

Table 2.3: Cross-sectional areas of different braid types.

# of core filaments	Take-up speed (mm/sec)	Braid angle	Cross-sectional area (mm^2)
3	3.99	11.2°	1.263
3	2.67	16.5°	1.282
3	2.00	21.5°	1.309
1	3.99	8.7°	0.979
1	2.67	12.8°	0.991
1	2.00	16.9°	1.007
0	3.99	6.9°	0.837
0	2.67	10.3°	0.845
0	2.00	13.6°	0.855
Single filament	-	-	0.139

where F is longitudinal force recorded by the load cell and A is the area as calculated via equation (2.8).

Outliers for elastic moduli and UTS values were determined. Interquartile range was multiplied by three in order to subtract from first quartile and to add to third quartile. The resulting lower and upper outer fence, respectively, were used to detect extreme outliers [38]. Extreme outliers for elastic modulus and UTS were eluded from further calculations.

2.5 Shape memory effect testing methodology

48 mm long specimens were prepared. 9 mm of masking tapes were applied on both ends of specimens to prevent unraveling, leaving a gauge length of 30 mm. Figure 2.7a, 2.7b, and 2.7c explain the temporary shape programming procedure which was conducted in Sun Electronics Systems ET2 Temperature Chamber with PC100-2 temperature controller that was attached to the tensile testing device. The chamber can be seen in Figure 2.6. Specimens

were clamped such that taped region would be inside the grips.

Before setting the temporary shape, the chamber was heated to 50 °C (T_g + 5 °C) at a rate of 1 °C/sec and held at this temperature for at least 3 minutes (Figure 2.7a). Specimens were elongated to 100% in strain, i.e. 30 mm at 0.2 mm/sec constant elongation rate (Figure 2.7b) and then cooled down with compressed air as soon as 100% strain was reached (Figure 2.7c). All shape recovery tests were conducted right after setting the temporary shape for each sample.

2.5.1 Shape recovery rate & maximum shape recovery

Figure 2.7d, 2.7e, and 2.7f explain the procedure followed in shape recovery rate and maximum shape recovery tests. After a specimen was programmed to its temporary shape (Figure 2.7b) and the chamber was cooled down (Figure 2.7c), an object with a small mass was attached to the braid to prevent curling. Amount of the attached mass was normalized with respect to the number of filaments in a braid, e.g. the braid with 3 core filaments had a total of 9 filaments and the attached mass was 19.74 g while the attached mass was reduced to 15.50 g for the braid with one core filament since it had 7 filaments in total. Amounts of the different masses are shown in Table 2.4. Temperature was increased to 50 °C to trigger the actuation (Figure 2.7d) and the braid started contracting due to SME (Figure 2.7e). Pictures were recorded with a Basler acA3800-10gm GigE camera at 5 Hz during recovery. An optical strain measurement technique was adopted to analyze recorded images, through which recovery rates, maximum strain recoveries, and shape fixities were obtained.

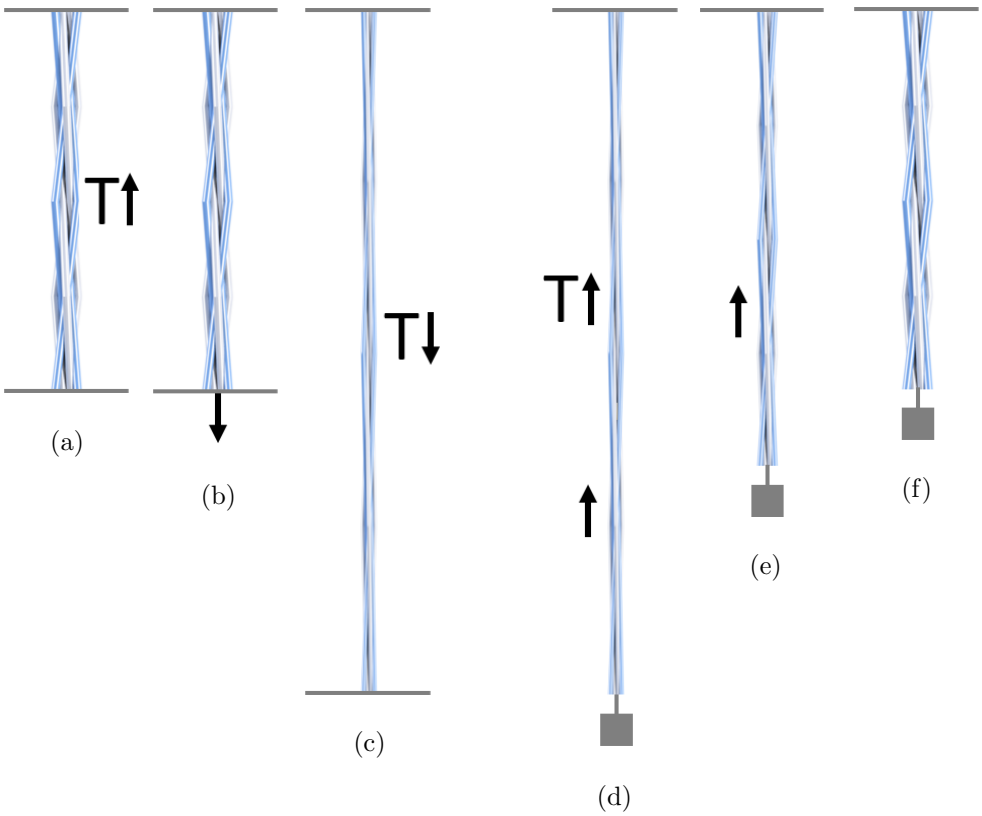

Figure 2.7: The procedure for setting the temporary shape and recovery test. (a) Sample was clamped and temperature was increased. (b) Braid was elongated at a constant rate at $T_g + 5\,^{\circ}C$. (c) Temperature was reduced to room temperature with forced air. (d) A small mass was attached to the braid and temperature was increased. (e) Braid started to contract and return to its original shape. This event was recorded for shape recovery rate, maximum shape recovery, and shape fixity analysis. (f) The tests were ended as the contraction stopped.

Table 2.4: Masses of the objects that were attached during recovery tests.

# of core filaments	Total # of filaments	Mass (g)
3	9	19.74
1	7	15.50
0	6	13.02
-	1 (single filament test)	2.40

Optical strain measurement

A custom script was written in Matlab R2018a to automate the analysis of images taken during recovery tests and it is provided in Appendix B. In this script; each image was loaded, unnecessary parts were cropped, and Prewitt edge detection algorithm was used to identify the edges [39]. This algorithm already exists inside Matlab's Image Processing Toolbox and can be applied with the `edge` command. An example untouched image, its cropped version, and the result after applying the edge detection algorithm can be seen in Figure 2.8. The `edge` command outputs a binary image in the form of a logical array in which elements of the array correspond to each pixel. The logical array's rows and columns represent the height and the width of an image, respectively. The columns were looped through one by one and all pixels between the first and last white pixel in a column were converted to white. Resulting image after this operation is shown in Figure 2.9.

Both ends of the braids had light-colored masking tapes on them. The tapes were wider than the braids as seen in Figure 2.8. Hence, the number of white pixels at the column which corresponded to the lower end of the braid was expected to have significantly more white pixels compared to the columns that had a part of the braid in them. A range of columns

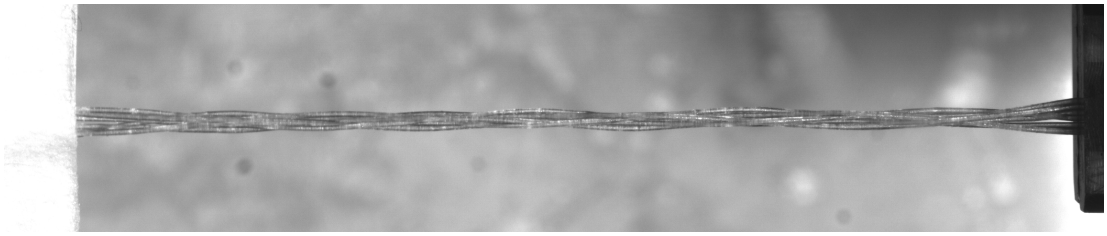

(a)

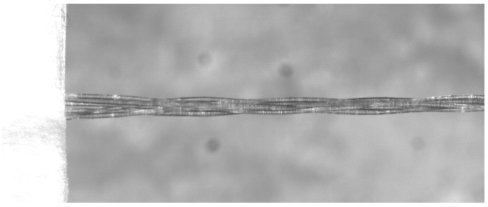

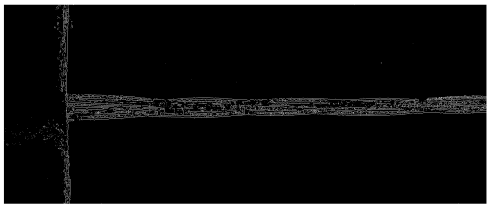

(b) (c)

Figure 2.8: An example image taken during shape recovery test. (a) Original (b) cropped version (c) after applying edge detection algorithm.

Figure 2.9: Resulting image when pixels between the edges along the height were marked white.

was designated to search for the boundary of the braid. If the image under investigation was the first of its set, the range consisted of all columns. The range was 50 pixels before and 300 pixels after the last detected boundary for the rest of the set. A threshold value was set and if the number of white pixels in three consecutive columns exceeded this threshold, the first of these three columns was chosen as the new boundary while scanning the columns from right to left in the designated search region. Figure 2.10 shows example images from the same set. Red lines indicate the programmatically detected boundary of the braids, whereas blue lines represent the number of white pixels in a column. The images on the right are the processed versions of their counterparts on the left.

The proportionality constant, C, between the two unit of measurements (pixels and milimeters) was found by placing a ruler into the frame. Change of length of the braid in each image, ΔL_i, was calculated from equation (2.10).

$$\Delta L_i = C\left(P_i - P_1\right) \tag{2.10}$$

where P_i is the braid boundary in each image and P_1 is the braid boundary in the first image of an image set. Unit of P is pixels, whereas ΔL_i is in milimeters.

The ends of the braids in the first image of a set were found manually with another Matlab script. Number of pixels between the ends was the initial length, P_{ini}. Although the braids were elongated until their length became 60 mm (100% in strain), the fixed elongation, L_f, was less than the original elongation (30 mm), L_o, because of the contraction that occured after the removal of the grips from the braids. L_f for each image set was calculated from equation (2.11).

$$L_f = P_{ini}\, C - L_o \tag{2.11}$$

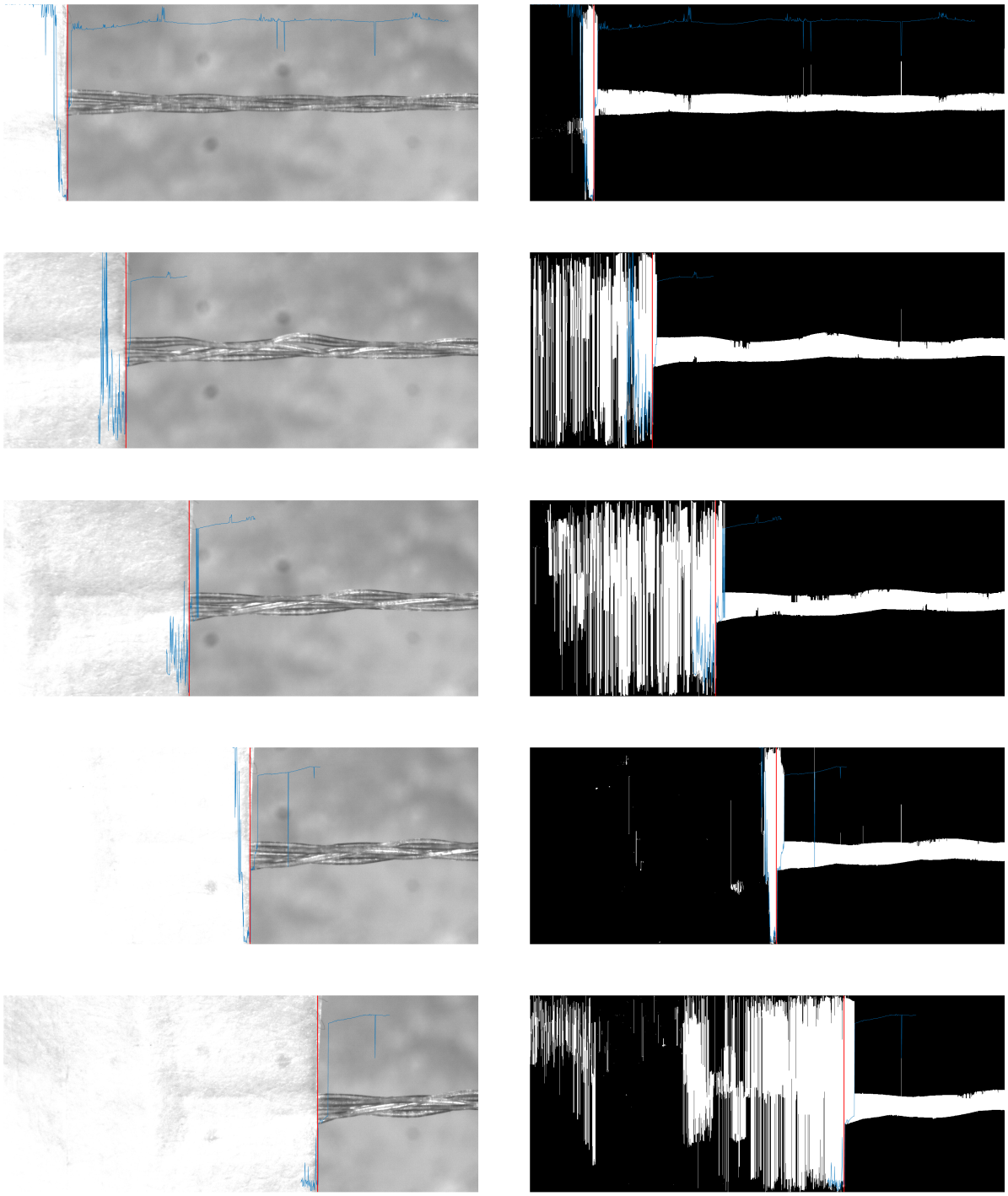

Figure 2.10: Example images during analysis from the same set. Red and blue lines represent the programmatically detected braid boundary and number of white pixels in columns, respectively.

The amount of recovered strain in each image, R_i, was found using equation (2.12).

$$R_i = \frac{\Delta L_i}{L_f} \tag{2.12}$$

The amount of fixed strain, i.e. shape fixity, R_F, was calculated for the braids with and without CNC content using equation (2.13).

$$R_F = \frac{L_f}{L_o} \tag{2.13}$$

2.5.2 Programming & recovery force measurement

Two types of force measurement were made; programming force and recovery force. Both tests were conducted on TA Instruments ElectroForce® 3200 Series III equipped with a 10 N load cell. Programming forces were recorded while setting the temporary shape with the methodology described above. A constrained recovery scenario was adopted in order to measure recovery forces. As the chamber cooled down to room temperature, stretched samples were clamped once again and temperature again was increased to 50 °C. This temperature was selected because it is slightly above T_g which is sufficient for actuation. Although 50 °C is above human body temperature, it is not enough to cause any harm to the skin unless the exposure is long. Therefore, 50 °C would be a suitable activation temperature for shape recovery to be actuated when the suture is applied to a human skin. Length of the specimens were held constant throughout the recovery. Forces were recorded for 1 minute while positions of the grips were fixed.

Chapter 3: Braided shape memory polymer surgical sutures[1]

The important properties of sutures include but are not limited to tensile strength, knot strength, tissue reaction, absorbability, and handling [40]. Moreover, a suture's stress-strain characteristics for both elastic and plastic deformations are key aspects of wound healing process. An optimal suture would have similar stress-strain behavior with the tissue that it is applied on [3, 4]. In the case of wound swelling, the suture would elongate and might be able to return to its original length depending on its elastic or plastic deformation characteristics [40]. Tensile strength represents the maximum stress a suture can hold without breaking and is one of the most important properties of sutures. Therefore, stress-strain behavior of a suture is essential for discovering properties such as elastic modulus, tensile strength or yield characteristics [41]. Since the proposed suture material under investigation is a SMM, SME features should also be examined. Speed of shape recovery, amount of recovered strain, and the force that the braid is able to apply during shape recovery are some of the primary characteristics that define the performance of SME.

The purpose of this chapter is to examine the effect of braiding parameters such as braid angle and existence/number of core filaments on the mechanical and shape recovery properties of the overall braided structure. For this purpose, three different take-up speeds were combined with changing number of core filaments. The braids were produced with take-up speeds of 2.00, 2.67, 4.00 mm/sec, while the number of filaments in the braid cores were 0, 1 and 3.

[1] A version of this chapter will be submitted to a scientific journal.

This experimental design resulted in nine different types of braids. Mechanical properties and SME characteristics of these braids were tested using the methodology described in Chapter 2. The performance of braided SMPU MM4520 as a suture material was assessed in comparison to elastic modulus and UTS values of some of the commercially available absorbable and nonabsorbable sutures. In addition, experimentally obtained elastic moduli were compared to analytically obtained results.

3.1 Mechanical properties in glass state

A representative stress-strain graph for the braids with different number of core filaments is shown in Figure 3.1. Slopes of the linear regions such as the ones presented in Figure 3.1 were used to calculate elastic modulus, whereas UTS values were calculated by finding the maxima of these curves. The stress-strain behavior was quite similar to previously reported tests which were conducted with the same/similar materials at comparable temperature and strain rate [9, 34]. Stresses increased linearly at a constant rate until reaching a yield point. Yield strains were higher for braids with larger braid angles. All braids deformed elastically at least until 3%, whereas this amount exceeded 4% for single filaments. Stress-strain curves of braids without a core filament and with one core filament showed more similarity compared to braids with three core filaments. Necking was observed in all samples after yield. Samples were elongated until they reached 90% strain and failure was not observed for any of the samples. Pictures of a representative test where the necking phenomenon can be observed are shown in Figure 3.2.

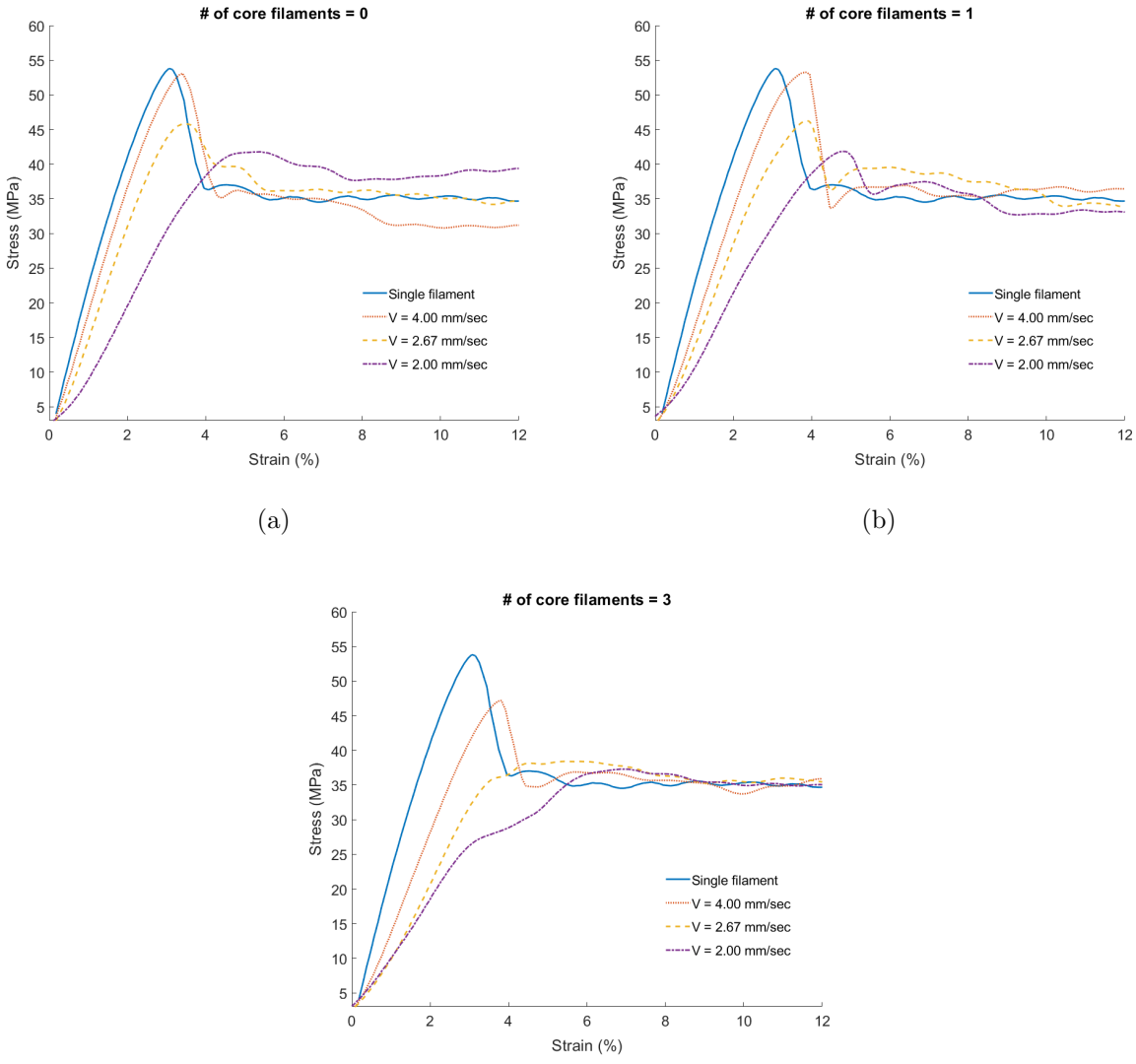

Figure 3.1: Representative stress-strain curves for the braids with (a) 0, (b) 1 and (3) core filament(s).

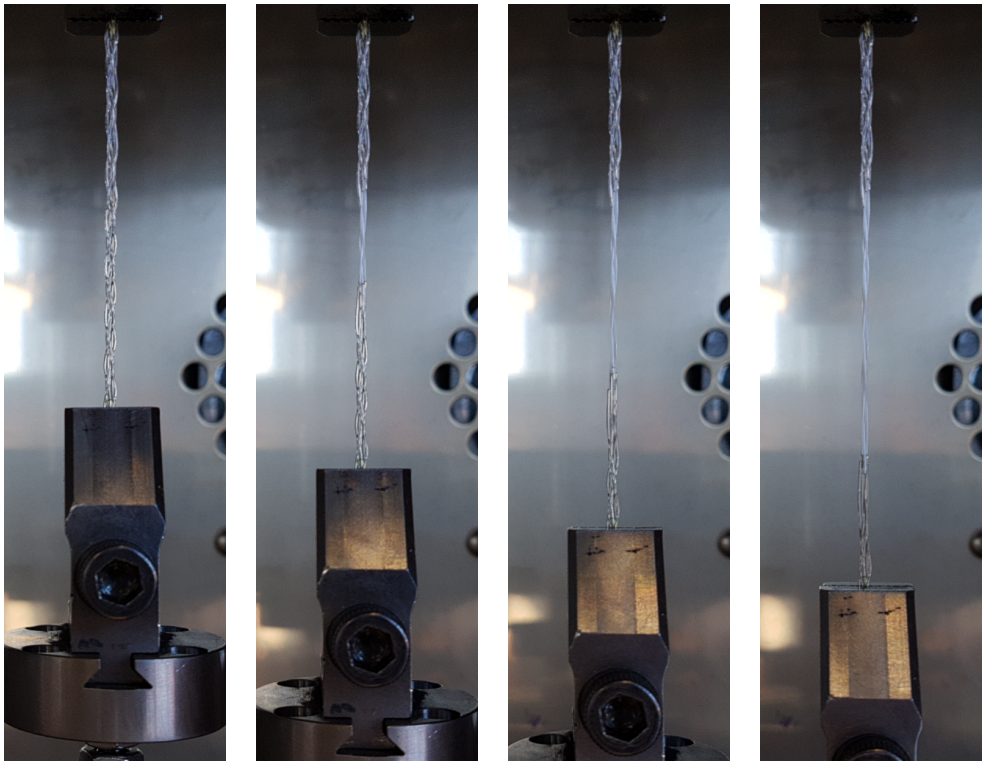

Figure 3.2: Images taken during a tensile tests.

3.1.1 Elastic modulus

Means and standard deviations of the elastic moduli for each braid type and single filament are presented in Figure 3.3 and the exact values are given in Table 3.1. Single filament tests yielded the highest elastic modulus (1.89 GPa), as expected [42]. Increasing braid angle reduced elastic modulus for each braid type, such that it decreased from 1.88 to 1.64 and 1.09 GPa for braids no core filaments, from 1.74 to 1.41 and 1.06 GPa for braids with one core filament, from 1.34 to 0.92 and 0.84 GPa for three core filaments, with increasing braid angle. This trend was also valid for the combinations of braids with no and core filament(s), i.e. elastic modulus values were 1.88 GPa for 6.9° braid angle, 1.74 GPa GPa for 8.7°, 1.64 GPa for 10.3°, 1.41 GPa for 12.8°, 1.09 GPa for 13.6°, 1.06 GPa for 16.9°; meaning that elastic modulus always decreased with increasing braid angle. However, the same argument cannot be made for the braids with three core filaments since elastic modulus of the braid with 11.2° braid angle was 1.34 GPa, whereas higher elastic moduli values were observed with higher braid angles and fewer core filaments. The same exception also existed for the braid with three core filaments and 16.5° braid angle. The reason behind might be the geometric asymmetry due to three core filaments, which did not exist for the braids with no and one core filament(s). Geometries at the sections where filaments interlace can be seen in Figures 2.3, A.1, and A.2.

A two-way analysis of variance (ANOVA) revealed that the main effects of number of core filaments ($p < 0.01$) and take-up speed ($p < 0.01$), as well as their interaction ($p < 0.01$) were highly significant. Significance of the interaction indicated that effect of the take-

up speed was also dependent on the effect of the number of core filaments, which can be explained by the fact that both take-up speed and number of core filaments contribute to the determination of braid angle which is one of the key braiding parameters affecting elastic modulus [43, 44].

Silk, polypropylene, polybutester, and nylon are some of the nonabsorbable suture materials [41]. Naleway et al. (2015) studied the mechanical properties of commercially available sutures produced with aforementioned materials and found that the elastic moduli for the sutures were 8.70, 0.75, 0.95 and 1.16 GPa for silk, polypropylene, polybutester and nylon, respectively, whereas most of the nonabsorbable suture materials had less elastic modulus [41]. In addition, Kreszinger et al. (2018) investigated absorbable monofilament sutures made of polyglyconate, polydioxanone, and chromic catgut [45]. Elastic modulus varied between 0.67 GPa and 1.57 GPa for these materials where the minimum and maximum were with polydioxanone and chromic catgut, respectively. Based on these values, it can be concluded that elastic modulus of braided SMPU MM4520 in this study is sufficient for a suture material. Moreover, it is possible to tailor the elastic modulus to a desired amount by modifying one or more braiding parameters such as filament diameter, take-up speed, number of core filaments, and braid angle.

The results were compared to the model presented in Handbook of Industrial Braiding by Ko et al. (1989) that can be used to predict a braid's elastic modulus [46]. Necessary properties for this model are longitudinal elastic modulus of the individual filaments, Poisson's ratio of the braid, and the volume ratios of undulating and core filaments. This model is applicable for tensile loading beyond jammed state which also requires knowing the braid angle at

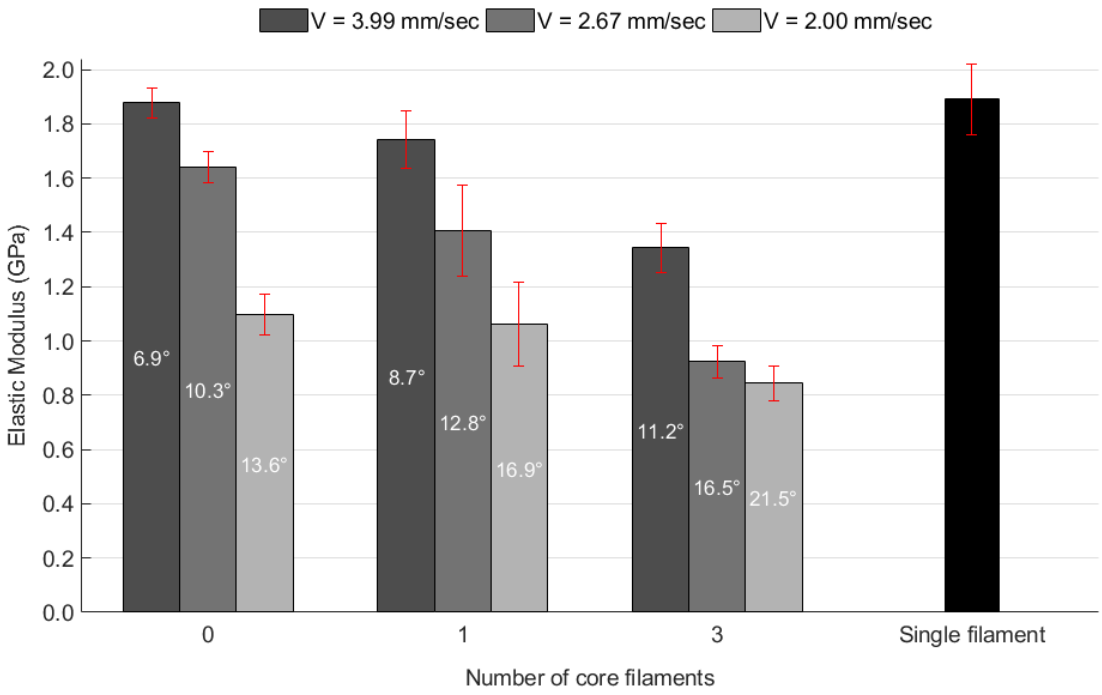

Figure 3.3: Mean and standard deviations of the elastic moduli. The numbers in the center of the bars represent corresponding braid angles. V is the take-up speed of the braider.

jammed state. In the present study, the angles from the geometric model were directly applied to the prediction model, i.e. these angles were assumed to be the braid angles at jammed state. Elastic modulus of the braid due to undulating yarns is given in equation (3.1).

$$E_{und} = E_f \, cos^2\theta \left(cos^2\theta - \nu \, sin^2\theta \right) \tag{3.1}$$

where E_{und} is the longitudinal elastic modulus due to undulating filaments, E_f is the longitudinal elastic modulus of the filaments, θ is the braid angle, and ν is the Poisson's ratio of the braid.

In order to account for the effect of core filaments on overall braid elastic modulus, a volume averaging method was applied. It was assumed that core filaments and the undulating filaments had equal strain at all times, which can be justified by the fact that both ends of the braid were tabbed with epoxy. Resulting elastic modulus of the braid is given by equation (3.2).

$$E_{braid} = V_{und} \, E_{und} + V_{core} \, E_{core} \tag{3.2}$$

where E_{braid} and E_{core} are the longitudinal elastic modulus of the braid and the core filaments, respectively. V_{und} and V_{core} are the volume ratios of undulating and core filaments, respectively. E_{core} in equation (3.2) is equal to E_f since core filaments are aligned with longitudinal axis of the braid. Volume ratios, V_{und} and V_{core}, are expressed in equation (3.3).

$$\begin{aligned} V_{und} &= \frac{N_{und}}{N_{und} + N_{core} \, cos\theta} \\ V_{core} &= \frac{N_{core} \, cos\theta}{N_{und} + N_{core} \, cos\theta} \end{aligned} \tag{3.3}$$

where N_{und} and N_{core} are the number of undulating and core filaments, respectively. Final expression for the elastic modulus of the braid is presented in (3.4), which is obtained by combining equations (3.1), (3.2), and (3.3).

$$E_{braid} = E_f \, cos\theta \, \frac{N_{und} \, cos\theta \left(cos^2\theta - \nu \, sin^2\theta\right) + N_{core}}{N_{und} + N_{core} \, cos\theta} \tag{3.4}$$

The Poisson's ratio, ν, in equation (3.4) is the ratio of percent change in braid diameter to the percent change in braid length, i.e. it is the Poisson's ratio of the braid as a structure. ν is assumed to be 0.5 as in Hristov et al. (2004) [47]. However, it was seen that a Poisson's ratio value of 5 was a better fit for most braid types. Elastic moduli found using equation (3.4) are presented in Table 3.1 which also includes the experimentally obtained values. These results are visualized in Figure 3.4 for ease of observation. From Figure 3.4, when ν is assumed to be 0.5, predicted elastic moduli are more accurate for fewer number of core filaments and/or smaller braid angles, which suggests that $\nu = 0.5$ tends to be more appropriate for such cases. This can be explained by the fact that filaments had less space to move in radial direction compared to braids with more core filaments and hence, reaching jammed state quicker. $\nu = 5$ seems to be a better assumption for most of the braid types although there is no previous literature to justify such a large value.

3.1.2 Ultimate tensile strength

UTS values were calculated from the stress-strain graphs obtained from experimental data such as the ones shown in Figure 3.1. Results are presented in Figure 3.5 and given individually in Table 3.1. General trend in UTS is similar to that of elastic moduli for all types of

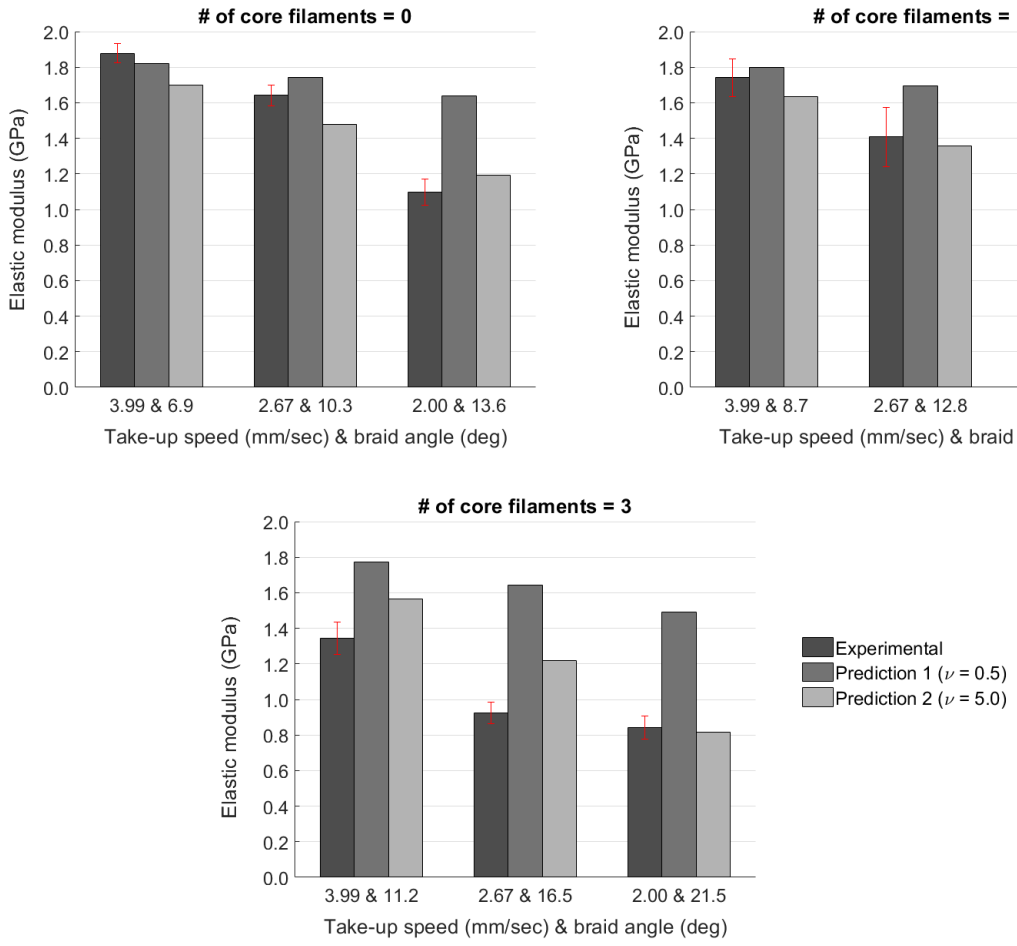

Figure 3.4: Experimental vs. predicted elastic moduli for the braids with different number of core filaments.

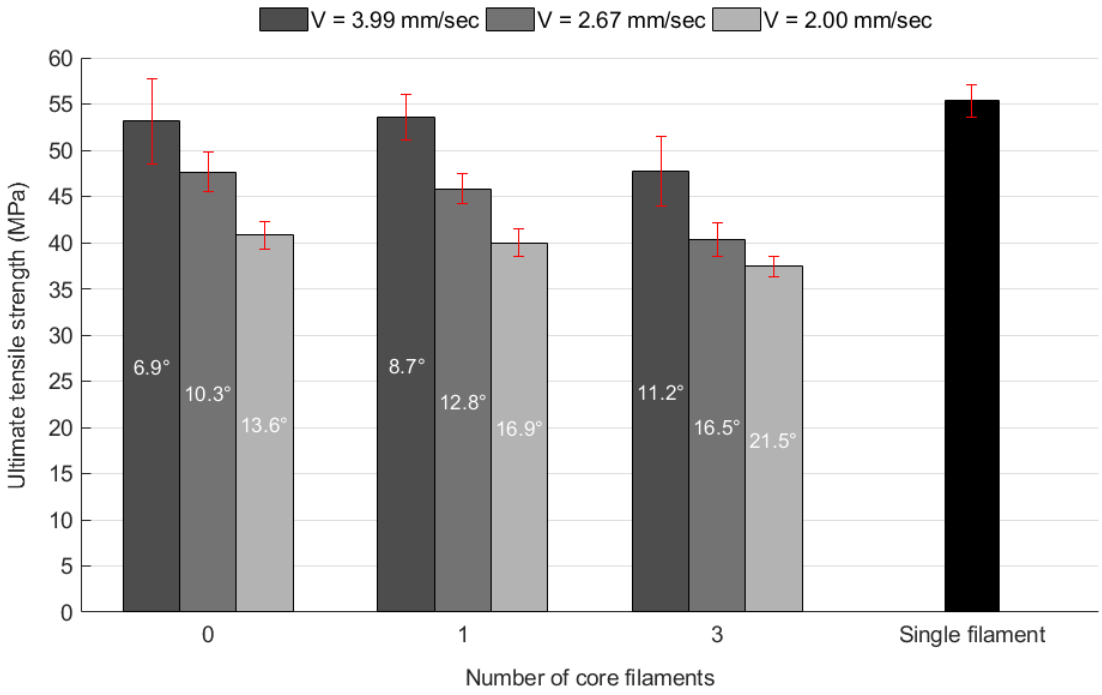

Figure 3.5: Mean and standard deviations of UTS. The numbers in the center of each bar represent the corresponding braid angle. V is the take-up speed of the braider.

braids, as indicated by the resemblance between Figures 3.3 and 3.5. Single filament had the highest UTS (55.36 MPa) compared to that of braids. Still, braids without a core filament and with one core filament that had low braid angles provided comparable strength to that of single filament. For example, average UTS was 53.12 MPa for the braids with no core filaments and 6.9° braid angle. In addition, braids with one core filament and 8.7° braid angle had an average UTS of 53.55 MPa. Both these UTS values were relatively close to that of single filament.

A two-way ANOVA with number of core filaments and take-up speed as the independent variables was performed. Main effects of both independent variables were significant with p-values less than 0.01. Their interaction ($p = 0.11$) was, however, not significant. When the

braids with equal number of core filaments were compared, UTS decreased with increasing braid angle, as expected [48]. Braids with more core filaments provided comparable strength to that of braids with fewer core filaments even though braid angles were larger, which suggests that axially aligned filaments had a considerable contribution to overall UTS. For example, braid angles for the braids with 3.99 mm/sec take-up speed were 6.9° and 8.7° for no axial filaments and for one axial filament, respectively. UTS was slightly higher when there was one axial filament (53.55 > 53.12 MPa). Similarly, braid angles were 13.6° for no core filaments and 16.9° for one core filament when the braids were produced with 2.00 mm/sec take-up speed. UTS values for these two were 40.79 and 40.00 MPa, respectively. Despite the clear difference in braid angles for these two configurations, difference in UTS values was very small.

From Naleway (2015), tensile strength of commercially available nonabsorbable sutures made of silk, polypropylene, polybutester and nylon were 1136.3, 493.1, 595.3 and 656.5 MPa, respectively, whereas minimum strength (410 MPa) was found for a absorbable suture made of chromic gut [41]. Stress-strain behavior of these sutures were different compared to the behavior of the braids in this study. The study does not mention to what degree the deformations were elastic, however stresses increased until failure and the curves did not show a yield point where the stresses decreased afterwards unlike the ones in this study. Another study made by Kreszinger et al. (2018) investigated absorbable monofilament sutures [45]. Minimum strength value was 212 MPa which was again for chromic catgut. Most of these values were approximately an order of magnitude higher compared to the SMPU MM4520 braids of this study. Means of increasing UTS of the braids should be further investigated

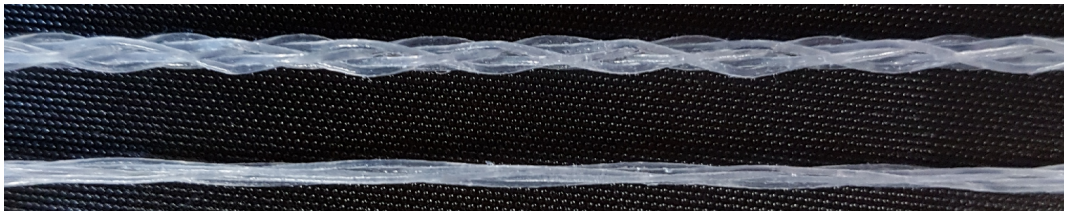

Figure 3.6: Original (top) and temporary (bottom) shape of a braid. The braid in this figure was produced at 2.67 mm/sec take-up speed without a core.

to obtain a comparable suture material.

3.2 Shape memory effect properties

Temporary shapes of filaments and braids were set following the exact same methodology for all types of SME tests. A picture of a braid before and after assigning a temporary shape is shown in Figure 3.6.

3.2.1 Shape recovery rate

Shape recovery rate and maximum strain recovery were analyzed using the optical strain measurement technique described in Chapter 2. An example set of images recorded during recovery tests is shown in Figure 3.8. A representative strain recovery curve with respect to time is given in Figure 3.7. The maximum slopes which also coincide with the linear regions of the curves as the ones shown in Figure 3.7 were considered as the recovery rate.

Results are shown in Figure 3.9 and tabulated in Table 3.2. Average recovery rates were close for the braids with same number of core filaments, whereas they decreased with increasing number of core filaments, such that the numerical values were 16.18, 16.34, and 15.11 %/sec

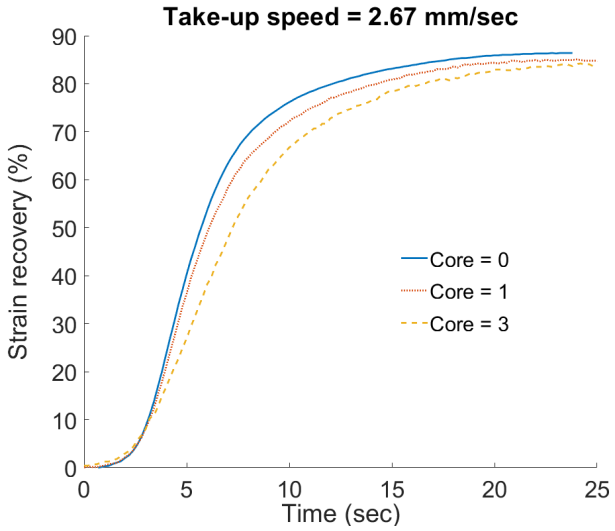

Figure 3.7: Representative strain recovery vs. time plots for the braids with various number of core filaments.

for the braids with no core filaments, 14.34, 14.68, and 14.96 %/sec for the braids with one core filament, 10.92, 11.45, and 11.99 %/sec for the braids with three core filaments. A two-way ANOVA showed that take-up speed was not significant ($p = 0.90$), whereas number of core filaments was highly significant ($p < 0.01$). Their interaction was also not significant ($p = 0.78$). Recovery rates were grouped by their number of core filaments and take-up speed, and are plotted in Figure 3.10 to visualize the significant effect of number of core filaments. Although number of core filaments was found to be a significant factor on recovery rate, the fact that take-up speed did not have any influence suggests that recovery rate does not change with braid angle because braid angle is a property determined by both take-up speed and number of core filaments. The clear pattern in Figure 3.10b indicates that number of filaments seems to affect recovery rate in a way that braids with fewer filaments recovered much faster.

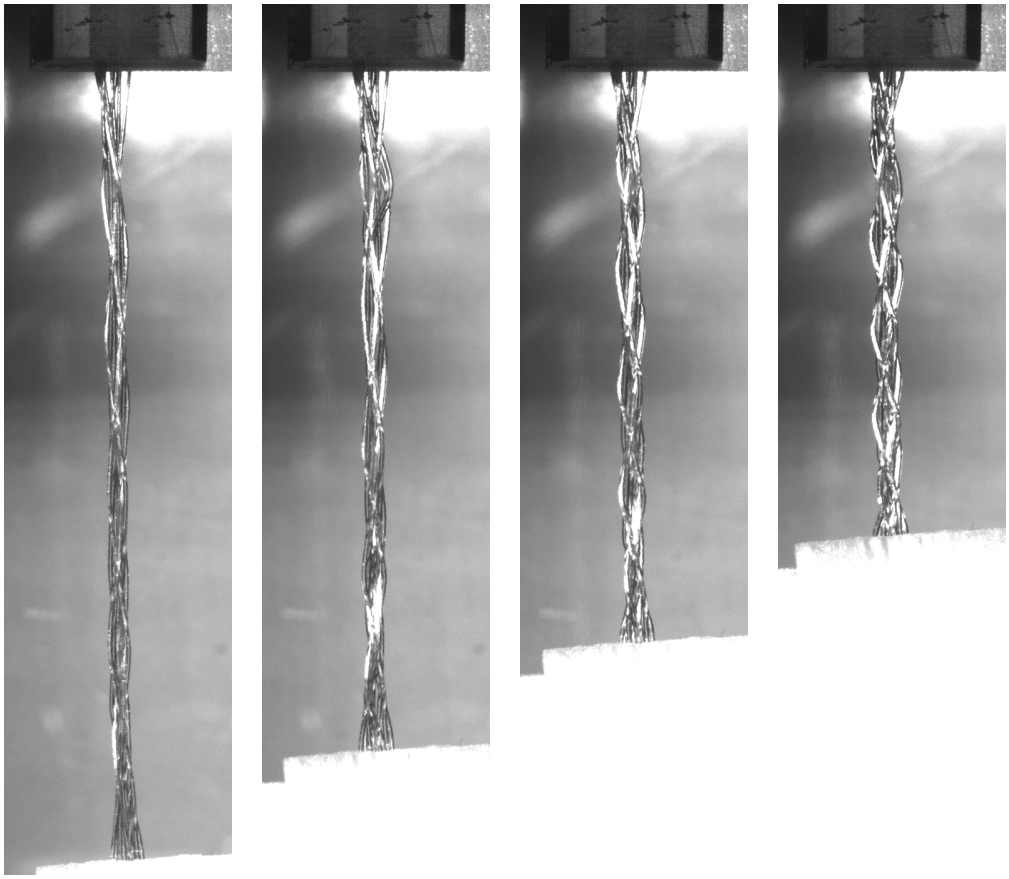

Figure 3.8: Example images recorded during shape recovery. Images are not successive.

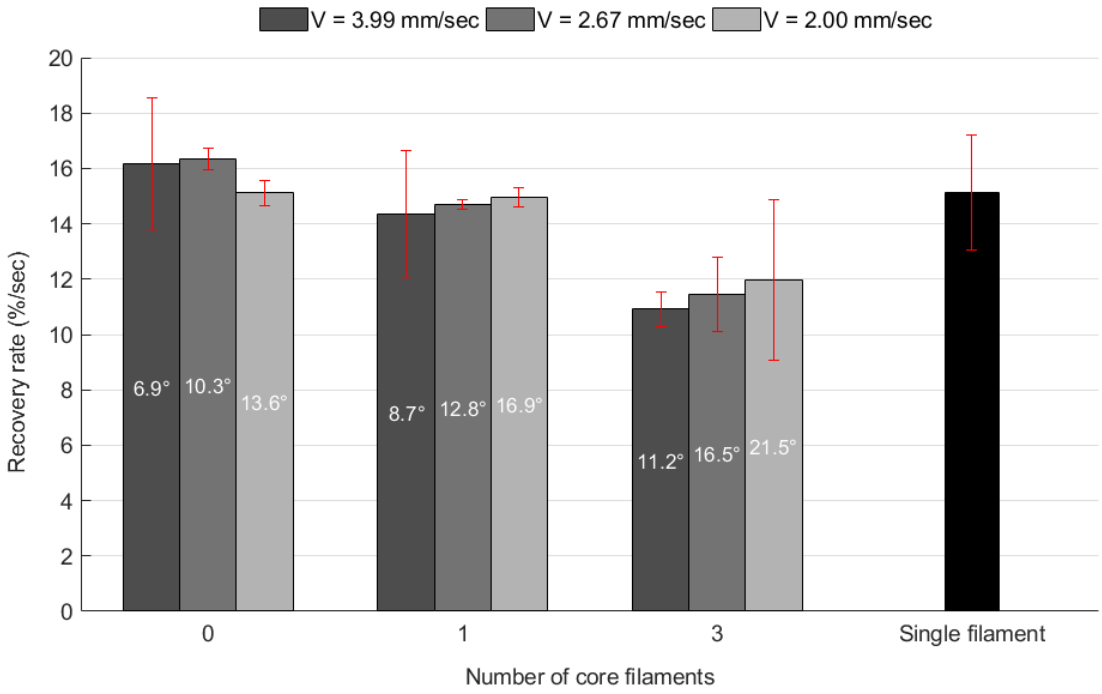

Figure 3.9: Mean and standard deviations of recovery rate. The numbers in the center of each bar represent the corresponding braid angle. V is the take-up speed of the braider.

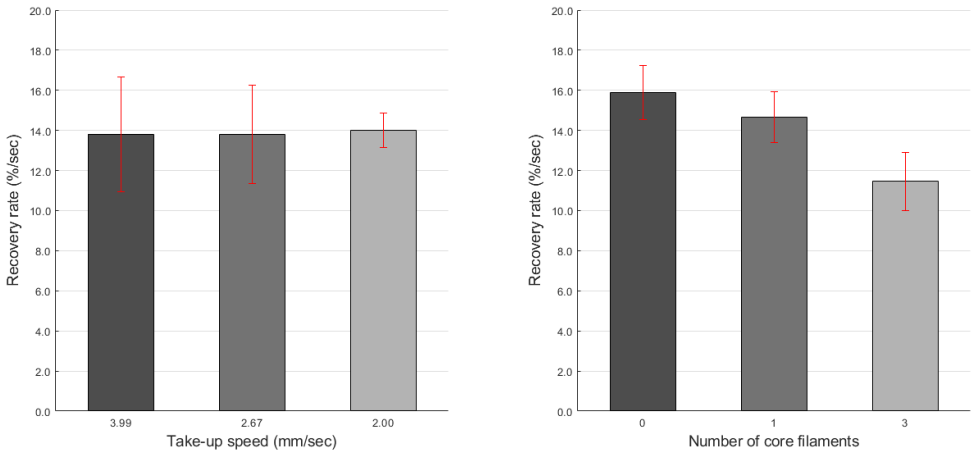

(a) (b)

Figure 3.10: Means and standard deviations of recovery rates grouped by (a) take-up speed, (b) number of core filaments.

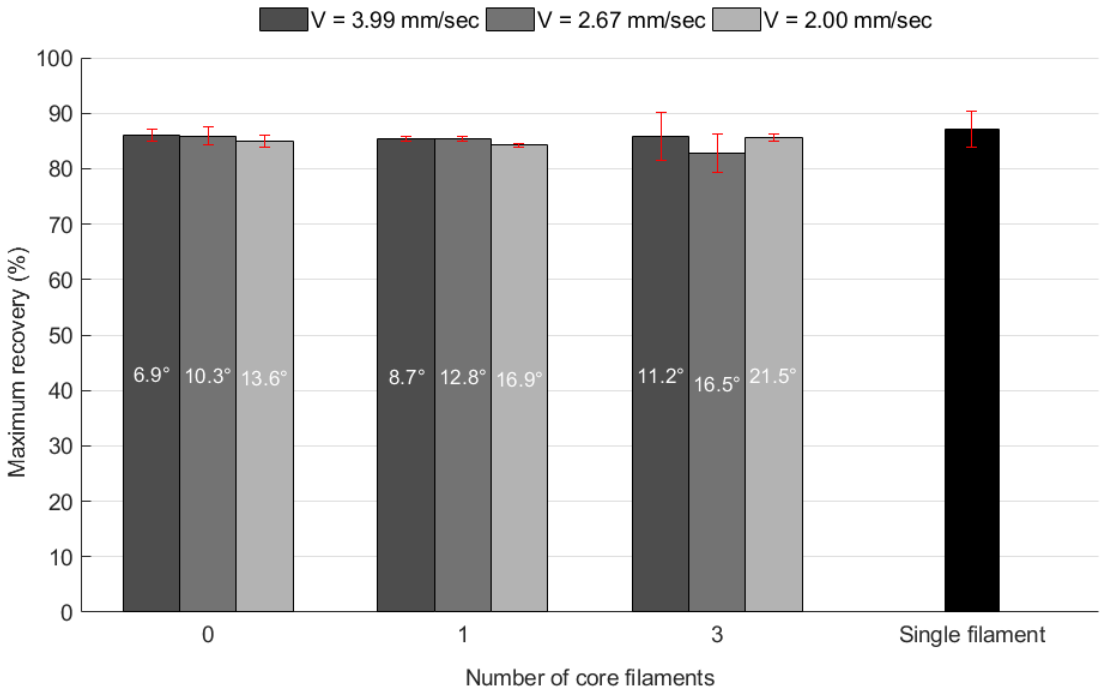

Figure 3.11: Mean and standard deviations of maximum shape recovery. The numbers in the center of each bar represent the corresponding braid angle. V is the take-up speed of the braider.

3.2.2 Maximum shape recovery

Maximum recovery that was reached in each strain recovery curve such as the ones given in Figure 3.7 was considered as the maximum recovered strain. Results of maximum shape recovery are presented in Figure 3.11 and Table 3.2. A two-way ANOVA revealed the p-values of 0.62 and 0.69 for take-up speed and number of core filaments, respectively, which suggests that neither were significant. Although the tests yielded less maximum recovery compared to previous literature [49], the recovery tests in this study cannot be considered as either perfectly free or constrained due to weight attachments.

The overall mean maximum recovered strain was 85.31% from which none of the braid configurations deviated significantly, whereas single filament had slightly higher maximum recovery (87.04%). Considering these results and small standard deviations, it is clear that number of core filaments, take-up speed, and braid angle were not significant factors in determining the maximum shape recovery.

3.2.3 Recovery force

A representative recovery force vs. time plot is given in Figure 3.12. Maximum forces that were reached in such plots were regarded as shape recovery force. The forces started to increase as soon as glass transition region was reached, made a peak and then dropped gradually due to stress relaxation, as seen in Figure 3.12.

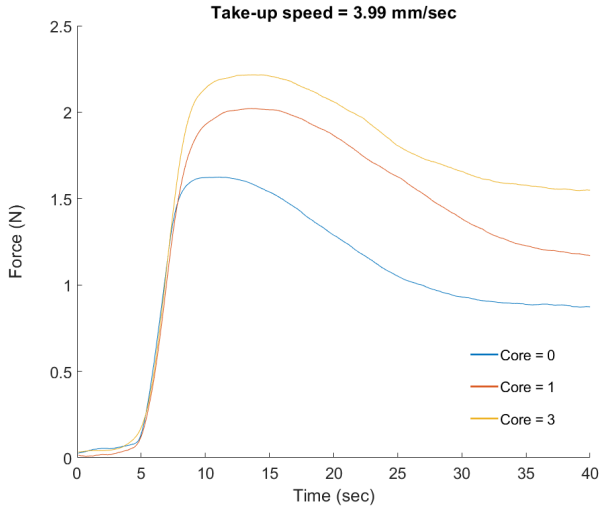

Figure 3.12: Representative force vs. time plots during constrained recovery.

Recovery forces recorded during experiments were divided by the area values given in Table 2.3 to find recovery stresses. Recovery forces are plotted in Figure 3.13. Numerical values

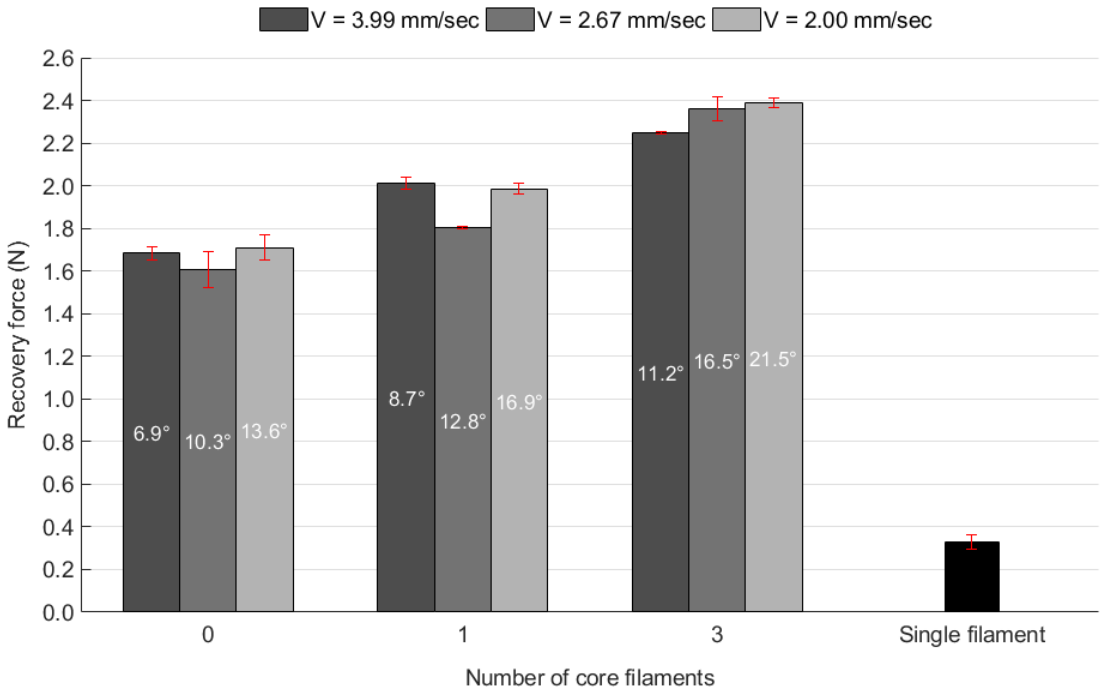

Figure 3.13: Mean and standard deviations of recovery force. The numbers in the center of each bar represent the corresponding braid angle. V is the take-up speed of the braider.

of the forces and stresses are given in Table 3.2. A two-way ANOVA was conducted on recovery force results. Number of core filaments had a significant effect on recovery force ($p < 0.01$), whereas take-up speed did not ($p = 0.11$), which is logical since it is expected for fewer filaments to exert less force. Recovery stresses for the braids with no core filaments (2.01 MPa for 6.9°, 1.90 MPa for 10.3°, 2.00 MPa for 13.6°) and one core filament (2.06 MPa for 8.7°, 1.82 MPa for 12.8°, 1.97 MPa for 16.9°) were similar, whereas it was slightly lower for the braids with three core filaments (1.78 MPa for 11.2°, 1.84 MPa for 16.5°, 1.83 MPa for 21.5°). Moreover, recovery stress for a single filament (2.38 MPa) was higher than that of braids.

3.3 Conclusion

Behavior of mechanical properties, namely, elastic modulus and UTS of braided SMP were similar, in a way that they both decreased with increasing braid angle. Prediction model for elastic modulus yielded relatively accurate results when Poisson's ratio was set to 5 for most type of braids, although a Poisson's ratio of 0.5 was more appropriate for some; the ones with fewer core filaments and small braid angles. This was explained by the jammed state assumption. Braid angles that were used in the prediction model were taken from the geometric models, however, they were not the braid angles at jammed state. As the number of core filaments and braid angle increased, braids would possibly have more space to move in radial direction, hence, greater Poisson's ratio values. Number of core filaments had an additional effect on UTS. When take-up speeds were the same for the braids with zero and one core filament(s), braid angles were smaller for the latter. However, UTS values of braids with one core filament were still comparable to that of braids with no core filaments due to existence of axial filament.

Number of core filaments affected shape recovery rate unlike take-up speed and braid angle which were found to be statistically insignificant, whereas none of the parameters was significant on maximum recovery. Recovery forces increased when more filaments were present in the braid as expected, whereas recovery stresses were the same for braids with no and one core filament(s). Braids with three core filaments exerted less recovery stress.

Elastic modulus of braided SMP were sufficient to be a suture material when compared to that of commercially available sutures. However, tensile strength of the sutures that are

currently in use were significantly higher compared to UTS values of braided SMP that were investigated in this study, by an order in most cases.

It was clear that room for improvement exists for both mechanical and SME properties, which was the focus of Chapter 4 where same properties were investigated for CNC reinforced SMP braids.

3.4 Tabulated results

The exact results of the tensile tests (elastic moduli, UTS) and shape recovery tests (recovery rate, maximum recovery, recovery force) are presented in Table 3.1 and Table 3.2, respectively, with the braid angles for each number of core filaments and take-up speed configuration.

Table 3.1: Tensile test results and elastic modulus predictions.

# of core filaments	Take-up speed (mm/sec)	Braid angle (deg)	Elastic modulus (GPa)				UTS (MPa)	
			Mean	Standard deviation	Predicted ($\nu = 0.5$)	Predicted ($\nu = 5.0$)	Mean	Standard deviation
3	3.99	11.2	1.34	0.09	1.77	1.57	47.74	3.75
3	2.67	16.5	0.92	0.06	1.65	1.22	40.31	1.82
3	2.00	21.5	0.84	0.07	1.49	0.82	37.40	1.05
1	3.99	8.7	1.74	0.11	1.80	1.64	53.55	2.51
1	2.67	12.8	1.41	0.17	1.70	1.36	45.83	1.62
1	2.00	16.9	1.06	0.15	1.56	1.00	40.00	1.49
0	3.99	6.9	1.88	0.06	1.82	1.70	53.12	4.61
0	2.67	10.3	1.64	0.06	1.74	1.48	47.64	2.12
0	2.00	13.6	1.09	0.08	1.64	1.19	40.79	1.53
Single filament	-	-	1.89	0.13	-	-	55.36	1.74

Table 3.2: Shape recovery test results.

# of core filaments	Take-up speed (mm/sec)	Braid angle (deg)	Recovery rate (%/sec)		Maximum recovery (%)		Recovery force (N)	Recovery stress (MPa)
			Mean	Standard deviation	Mean	Standard deviation		
3	3.99	11.2	10.92	0.62	85.73	4.32	2.25	1.78
3	2.67	16.5	11.45	1.34	82.79	3.56	2.36	1.84
3	2.00	21.5	11.99	2.90	85.59	0.72	2.39	1.83
1	3.99	8.7	14.34	2.30	85.39	0.49	2.01	2.06
1	2.67	12.8	14.68	0.17	85.38	0.40	1.81	1.82
1	2.00	16.9	14.96	0.34	84.25	0.31	1.99	1.97
0	3.99	6.9	16.18	2.39	86.05	1.09	1.68	2.01
0	2.67	10.3	16.34	0.40	85.92	1.56	1.61	1.90
0	2.00	13.6	15.11	0.44	84.93	1.07	1.71	2.00
Single filament	-	-	15.13	2.06	87.04	3.27	0.33	2.38

Chapter 4: Cellulose nanocrystal reinforced braided shape memory polymer surgical sutures[1]

In Chapter 3, the effect of the braiding parameters on the mechanical and SME properties of the braids was analyzed. In addition, the capability of braided SMPU of being a suture material was investigated by comparing the experimentally obtained results with the properties of sutures that are currently in use. The aim of this chapter is to investigate if the reinforcement of SMPU with CNC improves mechanical and SME properties of the braids. Previous studies reported better mechanical properties for CNC reinforced SMPU such as higher elastic modulus, tensile strength, and reduced creep and no improvements in SME [10, 50]. Studies also reported an improved shape recovery rate and no change in elastic modulus [36], whereas higher recovery forces were observed for silicon carbide particle reinforced SMPU [51]. In the light of the previous literature, mechanical and SME properties of the CNC reinforced SMPU composite filaments and braids were investigated similar to Chapter 3. All tests were conducted with 10 samples for each CNC wt% (0.5, 2.0, 4.0). Most of the tests were not repeated for neat SMPU (0.0 wt% CNC), rather the results from Chapter 3 were used.

[1] A version of this chapter will be submitted to a scientific journal.

4.1 Mechanical properties in glass state

Representative stress-strain curves for the braids with different CNC wt% are given in Figure 4.1a. Elastic modulus and UTS values were calculated from such curves as previously done in Chapter 3. The original length of the samples was 50 mm and some of them were elongated to 95 mm (90% in strain) to detect a possible failure. None of the samples failed until 90% strain and further elongations could not be observed due to machine limitations and low strain rate. Higher strain rates could possibly result in failure before 90% strain [34]. Representative stress-strain curves for the braids that were elongated to 90% in strain are shown in 4.1b. Curves showed a typical flexible plastic behavior; started with a linear region of elastic deformation, reached a yield point followed by plastic deformation. Braids without CNC content had higher stress levels throughout the tests although the overall behavior was similar across all types. Numerical values of the results discussed in this section are presented in Table 4.1.

4.1.1 Elastic modulus

Elastic moduli of the braids and filaments that were produced with different CNC wt% are presented as a bar graph in Figure 4.2. A one-way ANOVA was conducted on the results. P-values were 0.03 and 3.27E-06 for filaments and braids, respectively, which suggested a significant difference between the elastic moduli of different CNC wt%. Box plots of the results were given in Figure 4.3. From these box plots, it can be concluded that elastic moduli of filaments and braids without CNC content differed from the rest. Another one-

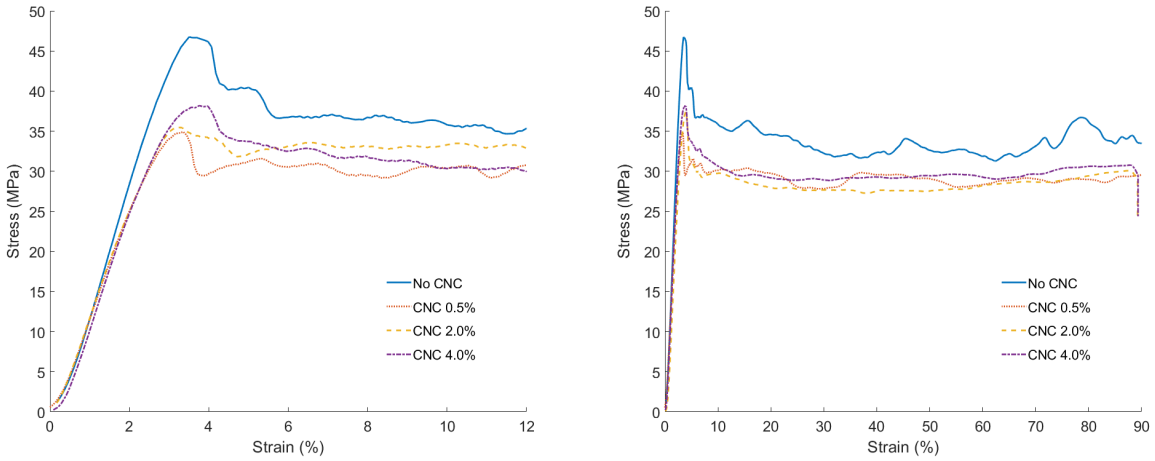

(a) (b)

Figure 4.1: Representative stress-strain curves for braids with different CNC wt% until (a) 12% strain and (b) 90% strain.

way ANOVA was conducted by excluding 0.0 wt% to test this claim. P-values were 0.56 and 0.13 for filaments and braids, respectively, meaning that elastic modulus decreased with CNC addition although the amount of CNC content did not matter for this change. The overall average decrease in elastic modulus with CNC addition was 8.2% for filaments and 11.7% for braids.

While some studies on CNC reinforced SMPU reported an increase in elastic modulus when CNC reinforcement is present [10, 50], another study reported that it had no effect [36]. Particle dispersion might be the underlying reason behind these contradictory findings. Dispersion is an important aspect of polymer-matrix nanocomposites, which influences mechanical properties greatly through distribution and agglomeration [10]. In the case of poor interfacial adhesion between polymer matrix and reinforcing nanoparticles, agglomerated CNC particles can behave as a gap inside polymer matrix, resulting with a lower elastic modulus

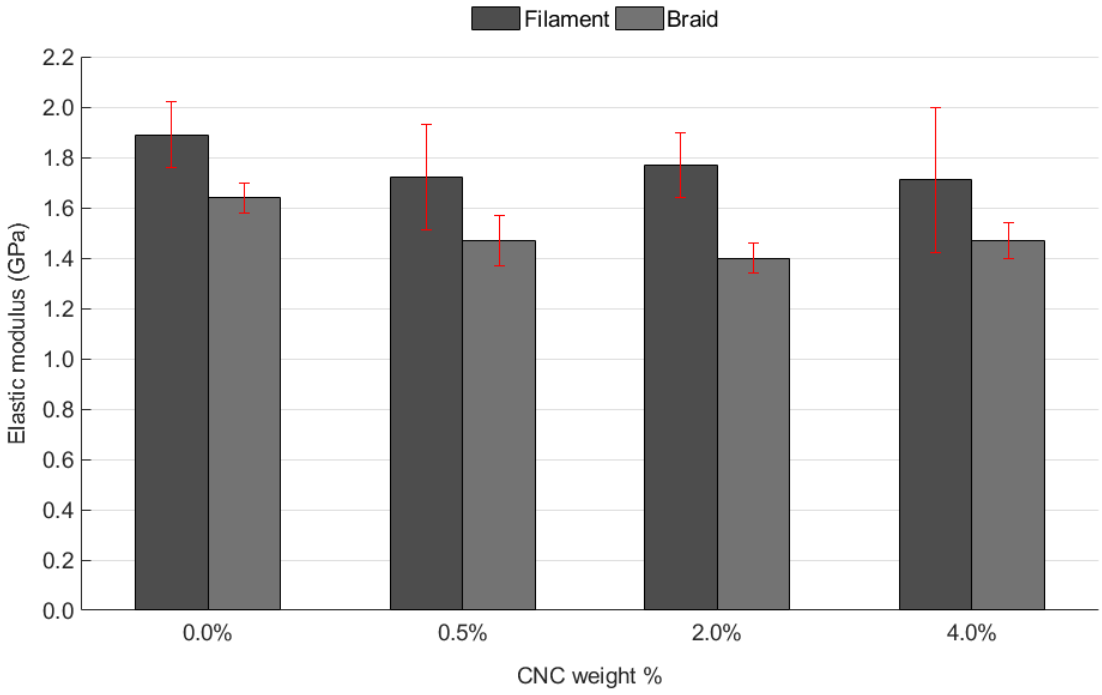

Figure 4.2: Elastic moduli of filaments and braids with different CNC wt%.

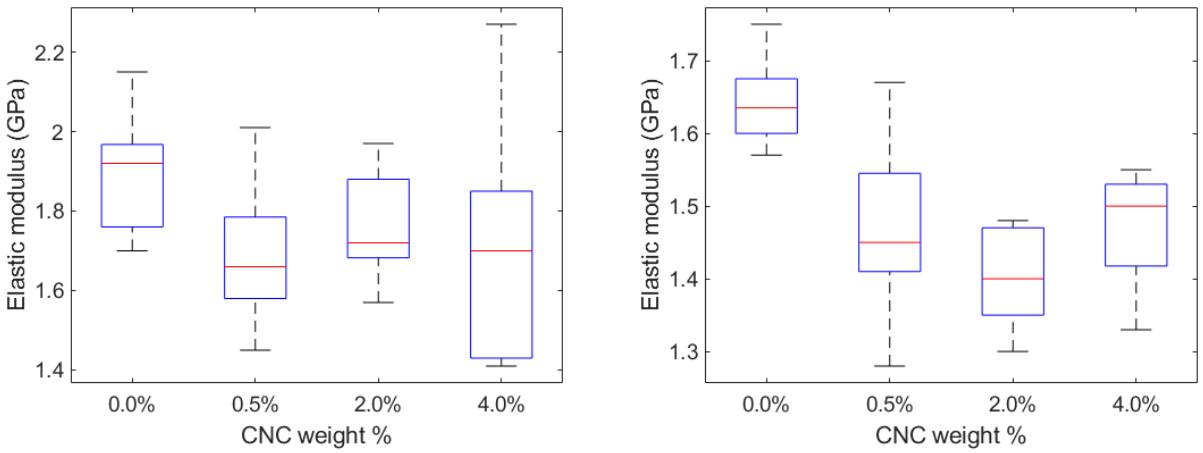

(a) (b)

Figure 4.3: Box plots for elastic moduli of (a) filaments and (b) braids for different CNC wt%.

in that region. Hence, poor dispersion and interfacial adhesion might be the driving forces behind the effect of CNC reinforcement on elastic modulus.

Some typical values for absorbable and nonabsorbable sutures were discussed previously in Section 3.1.1. Even though CNC had a negative effect on the elastic modulus of the braids, these values are still comparable and sometimes much higher relative to that of commercially available sutures [41, 45]. These results showed that braided CNC reinforced SMPU MM4520 is suitable as a suture material in terms of elastic modulus. In addition, it is possible to obtain a desired elastic modulus by changing braiding parameters.

4.1.2 Ultimate tensile strength

Bar graph for UTS values for the filaments and braids with different CNC wt% is presented in Figure 4.4. A trend similar to elastic modulus can also be seen for UTS. Therefore, same statistical methodology was applied to UTS test results as well to see if the amount of CNC had a significant effect on UTS. One-way ANOVA revealed the p-values of 9.91E-07 and 1.06E-13 for filaments and braids, respectively, meaning that UTS values were significantly different for different CNC wt%. Box plots are shown in Figure 4.5. As seen in the box plots, almost all test data for the filaments with no CNC content yielded a higher UTS value compared to filaments with CNC content. This behavior was clearer for braids, such that none of the UTS values for braids with CNC content surpassed the UTS of the braids without any CNC content. One-way ANOVA was conducted for 0.5, 2.0 and 4.0 CNC wt%, and the p-values were 0.29 for filaments and 0.76 for braids. It can be concluded that addition of CNC resulted with a decrease in UTS, however, the amount of CNC did not have a significant

effect. The UTS drop was 16.6% for filaments and 22.2% for braids. Effect of CNC was much more significant for UTS compared to elastic modulus.

Some typical tensile strength values for sutures were mentioned previously in Section 3.1.2. UTS of the braids produced with neat SMPU was significantly less than the commercially available sutures as mentioned in Chapter 3 and it dropped further with CNC reinforcement. One of the goals of reinforcing SMPU braids with CNC was to increase the overall strength. Previous studies showed that tensile strength of SMPU increased when reinforced with CNC [10, 50]. The reason behind the drop in UTS in this study might be bad dispersion. Agglomeration and non-uniformity of nanoparticles inside the polymer matrix can cause crack initiation and propagation due to stress concentrations which would result in low strength compared to that of neat polymer matrix [10, 52]. This was proven to be the case for carbon nanotube reinforced polymers [53, 54]. Therefore, dispersion of CNC reinforced SMPU should be improved to obtain comparable strength to that of sutures currently in use.

4.2 Shape memory effect properties

SME properties were found through thermomechanical experiments by following the methodology described in Chapter 2. The amount of fixed strain, i.e. shape fixity and programming stresses (stresses on the braid while setting the temporary shape when the material is in rubbery state) was also presented in addition to the SME tests in Chapter 3. Numerical values of the SME properties discussed in this chapter are shown in Table 4.2 and 4.3.

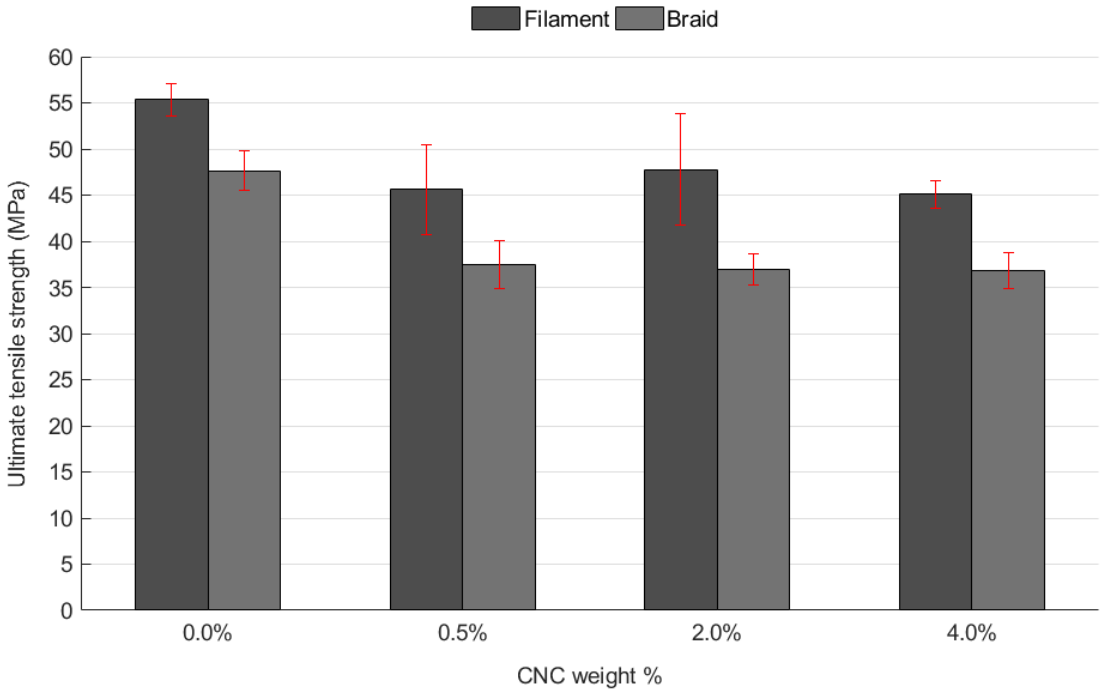

Figure 4.4: UTS of filaments and braids with different CNC wt%.

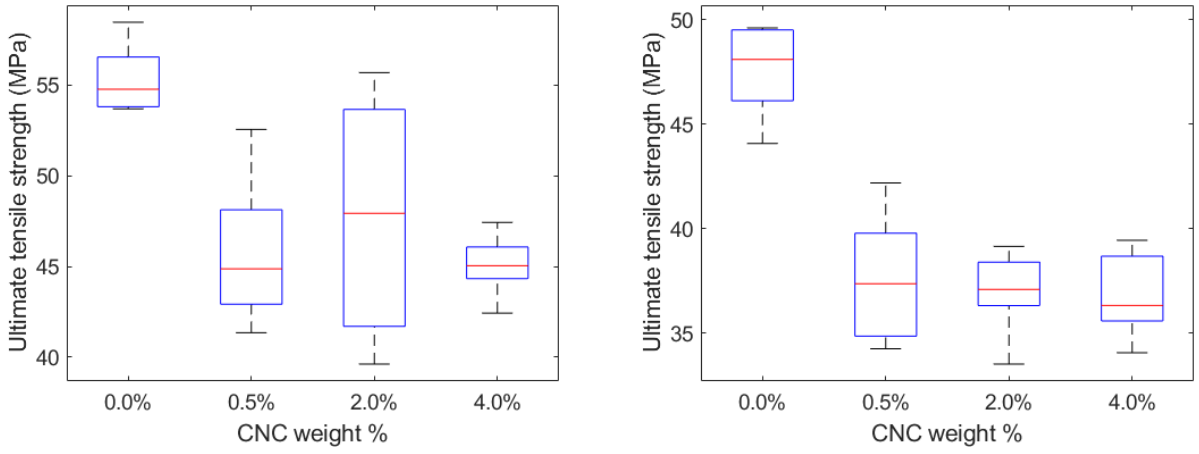

(a) (b)

Figure 4.5: Box plots for UTS of (a) filaments (b) braids for different CNC wt%.

4.2.1 Shape fixity

All samples were elongated to 100% in strain, i.e. their length changed from 30 mm to 60 mm. They were cooled down as soon as the length of the braid reached 60 mm. Although a minor amount of stress relaxation occurred during cooling down, the stress of the braids never dropped to zero. Due to non-zero stress, the braids contracted as they were relieved from the grips. The amount of contraction was very small for the braids in previous chapter (Chapter 3). However, there were visible contractions for the braids with CNC content. Shape fixities were calculated using equation (2.13) and are shown in Figure 4.6. Fixed elongation was 29.11 mm (97.04%), 28.34 mm (94.46%), 27.32 mm (91.05%), and 27.11 mm (90.36%) for 0.0, 0.5, 2.0 and 4.0 wt% CNC, respectively. From these results, it is clear that the amount of CNC had a negative effect on shape fixity.

4.2.2 Shape recovery rate

Test results for shape recovery rate were shown in Figure 4.7. Although recovery rate was smaller for 0.5 wt% (14.56 %/sec) compared to 0.0 wt% (15.88 %/sec), there was a slight improvement for 2.0 wt% (17.47 %/sec) and 4.0 wt% (17.72 %/sec).

4.2.3 Maximum shape recovery

Maximum shape recoveries are presented in Figure 4.8. The overall trends were similar for maximum shape recovery and recovery rate. Maximum shape recovery was one of the SME

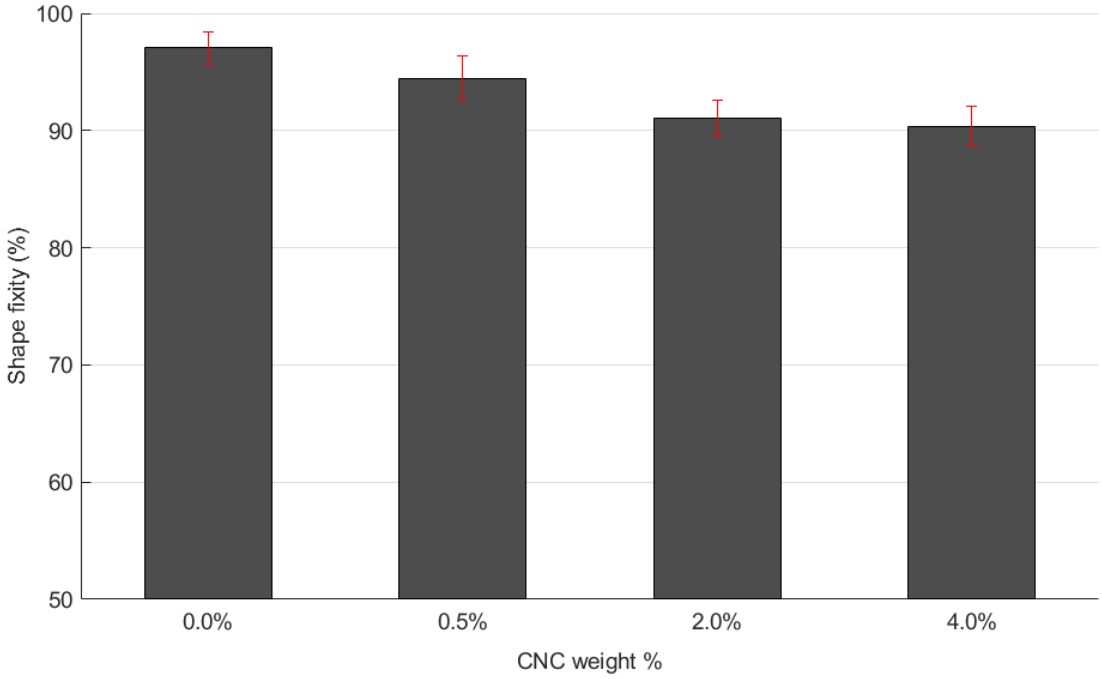

Figure 4.6: Shape fixities of braids with different CNC wt%.

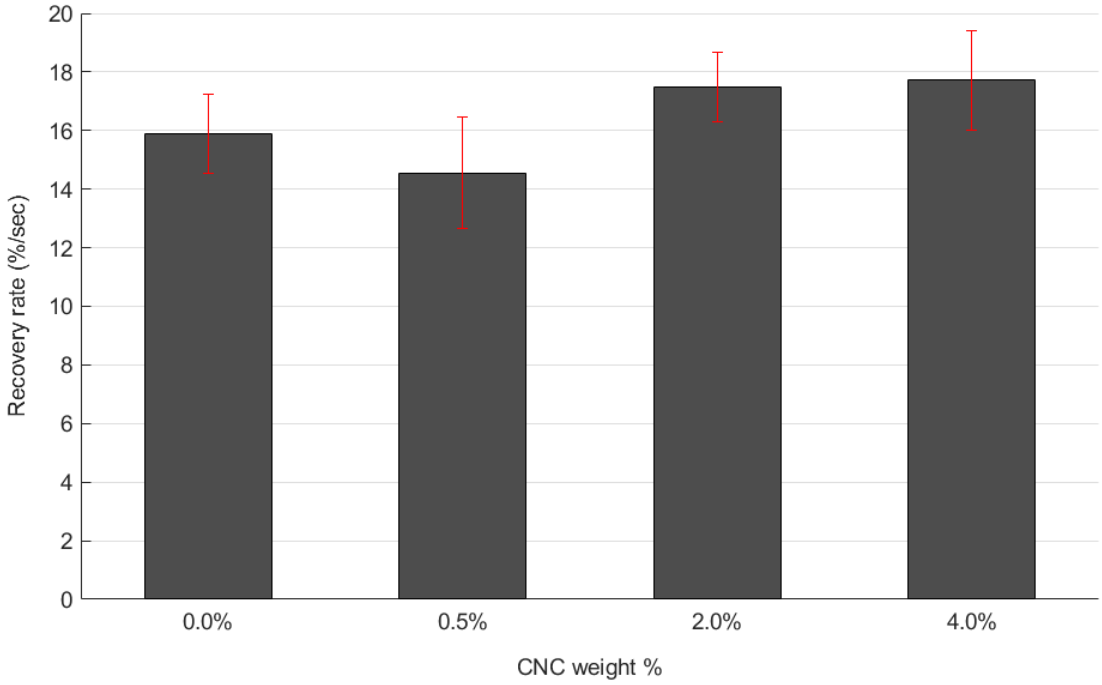

Figure 4.7: Shape recovery rates of braids with different CNC wt%.

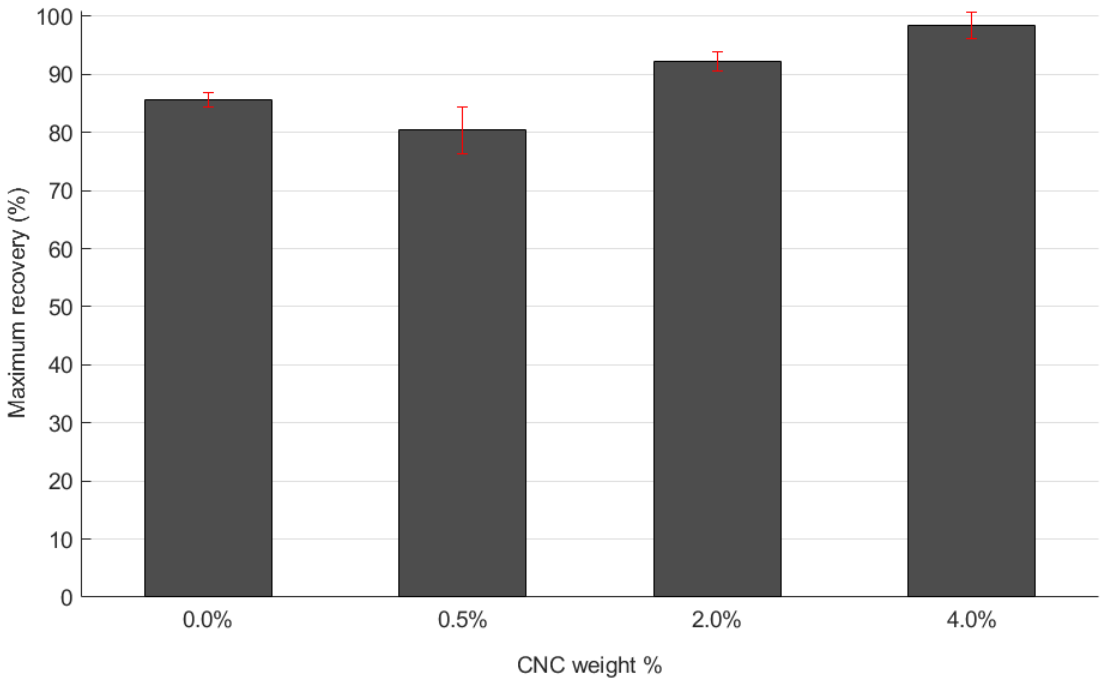

Figure 4.8: Maximum recovered strain of braids with different CNC wt%.

features where higher CNC wt% had a substantial contribution. Even though braids with 0.5 wt% CNC (80.36% maximum recovery) did not show a better performance compared to braids with no CNC content (85.63%), maximum recovery values were much higher for 2.0 and 4.0 wt% (92.28% and 98.40%, respectively). The maximum recovery peaked for the braids with 4.0 wt%, such that they almost fully recovered. It should be noted that all braids had approximately 13 g of mass attached to their bottom during the recovery to prevent curling, which might have reduced the amount of recovery.

4.2.4 Recovery stress

Representative recovery stress vs. time curves are given in Figure 4.9. The maximum stresses in such curves were regarded as the recovery stress. The overall trend in all curves were

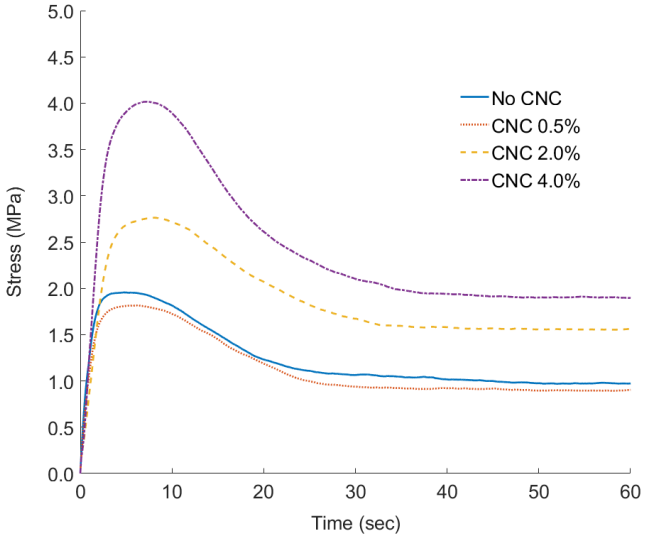

Figure 4.9: Representative recovery stress vs. time curves for braids with different CNC wt%.

similar. There was a sharp increase in stress as soon as temperature was increased although their slopes slightly varied. The increase in stress ended with a peak and then stresses dropped due to stress relaxation. Even though the amount of time it took to reach a peak was not the same for different CNC wt%, it was always less than 10 seconds. Approximately 50% of the maximum recovery stress was preserved at 60 second mark after actuation in all cases.

The results for maximum recovery stresses can be seen in Figure 4.10. Among all SME features, recovery stress was the one where CNC addition excelled the most. Braids with 0.5 wt% CNC showed poor performance compared to the braids with no CNC content as previously seen in shape recovery rate and maximum shape recovery. However, both 2.0 wt% and 4.0 wt% CNC exerted higher forces during recovery. The average values for recovery stress were 2.53 and 4.03 MPa. These values indicated an increase of 25.9% and 100.5%,

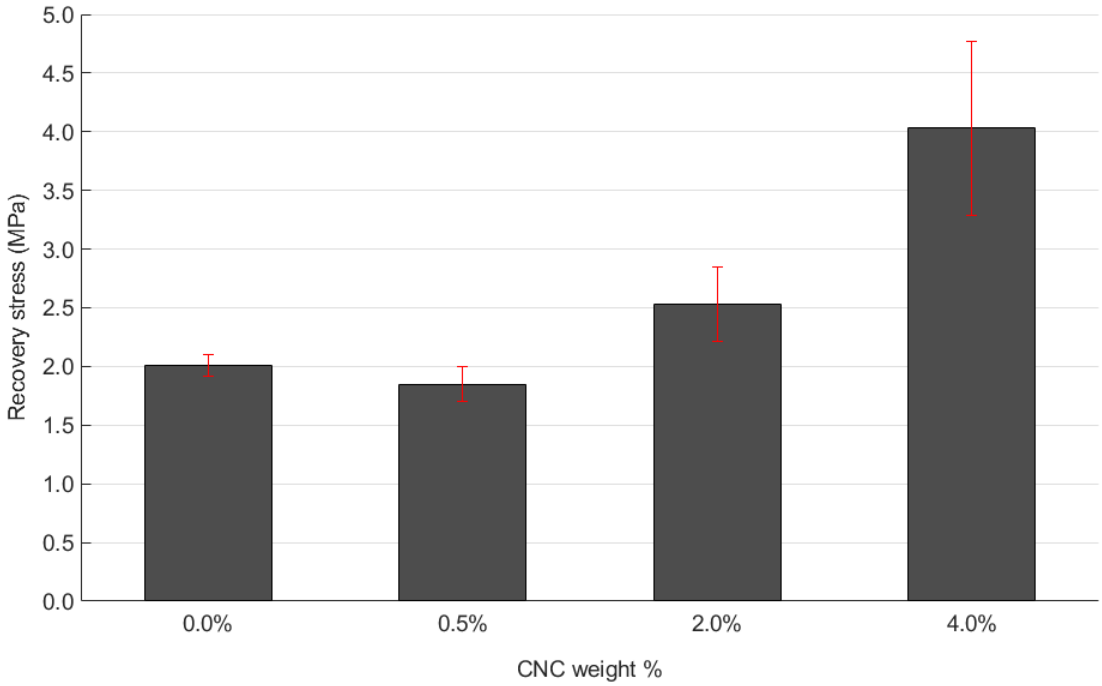

Figure 4.10: Maximum recovery stresses of braids with different CNC wt%.

respectively, when compared to the braids with no CNC content.

Lendlein (2002) produced a SMP monofilament suture with a diameter of 1 mm, which was able to generate 1.6 N during recovery in vitro meaning a recovery stress of 2.04 MPa [2]. SMP braids produced in this study with 2.0 and 4.0 wt% CNC both exceeded this value by a substantial amount, proving the impact of CNC. It should be noted that although the SMP suture was elongated 200% in strain in Lendlein (2002), recovery stress value was quite close to the recovery stresses of braided SMPU with no CNC content produced for this study.

4.2.5 Programming stress

Stresses on the braids were recorded while setting temporary shapes for SME tests. A representative stress-strain curve is shown in Figure 4.11. All braids had substantially less stress (by approximately an order lower) compared to mechanical tests in glass state (Section 4.1) because temperature of the braids was above T_g and consequently, they were in rubbery state. Stress levels were similar for all CNC wt% for low strains. After about 30% strain, higher stresses were observed for braids with 2.0 and 4.0 wt% CNC compared to 0.0 and 0.5 wt% CNC. Slopes of the stress-strain curves of the braids with 0.0 and 0.5 wt% CNC decreased throughout the tests, whereas they remained constant, or increased even after strain levels of 50% for the braids with higher CNC wt%. Final programming stress values when 100% strain was reached were close to maximum recovery stress. The average maximum programming and recovery stresses were 1.89 and 2.01 for 0.0 wt%, 1.77 and 1.85 for 0.5 wt%, 3.05 and 2.53 for 2.0 wt%, 4.60 and 4.03 for 4.0 wt%, respectively, which indicated that both programming and recovery stresses showed the same overall trend with changing CNC wt%.

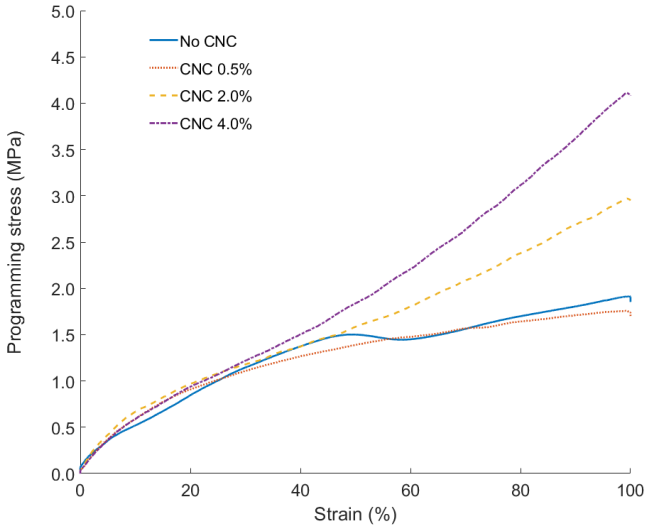

Figure 4.11: Representative programming stress-strain curves of braids with different CNC wt%.

4.3 Conclusion

Both elastic modulus and UTS decreased with the addition of CNC, however, the amount of CNC wt% did not influence this reduction. UTS showed a higher decrease compared to elastic modulus for the braids (11.7% vs. 22.2%), which was linked to poor dispersion of CNC inside SMP.

Braids with 2.0 and 4.0 wt% CNC demonstrated much better performance for all SME properties compared to braids with 0.0 and 0.5 wt% CNC. Shape recovery rate, maximum amount of recovery, maximum recovery stress, and maximum programming stress all showed the same pattern for different CNC wt%. Therefore, a generalization about SME properties can be made at this point, meaning that all these aforementioned properties behave in a way that they all either increase or decrease for a specific CNC wt%. This statement can almost

be extended for shape fixity too, except for the braids with 0.5% CNC where this pattern did not apply as seen in Figure 4.6.

Improved SME characteristics could be asserted to the high elastic modulus of CNC particles. Elastic strain stored in the CNC particles was frozen after temporary shape was set due to polymeric matrix; and because of its high modulus, it applied a much higher force to regain its original shape of the elastically deformed portion [36], which would explain higher recovery forces and rates. The elastic deformation of CNC that could not be frozen inside the polymeric matrix possibly lowered the shape fixity and hence shape fixity reduced with increasing CNC wt%.

4.4 Tabulated results

All the results discussed so far in Chapter 4 are presented in table form. Table 4.1 shows the results for tensile tests while the material was in glass state, whereas results of the tests related to SME are given in Table 4.2 and 4.3.

Table 4.1: Tensile test results of the filaments and braids with CNC content.

CNC wt% ratio	Type	Elastic modulus (GPa)		UTS (MPa)	
		Mean	Standard deviation	Mean	Standard deviation
0.0	Filament	1.89	0.13	55.36	1.74
0.5	Filament	1.72	0.21	45.61	3.15
2.0	Filament	1.77	0.13	47.76	6.02
4.0	Filament	1.71	0.29	45.07	1.50
0.0	Braid	1.64	0.06	47.64	2.12
0.5	Braid	1.47	0.10	37.46	2.61
2.0	Braid	1.40	0.06	36.95	1.65
4.0	Braid	1.47	0.07	36.82	1.90

Table 4.2: Shape recovery rate and maximum recovery of the braids with CNC content.

CNC wt% ratio	Recovery rate (%/sec)		Maximum recovery (%)	
	Mean	Standard deviation	Mean	Standard deviation
0.0	15.88	1.36	85.63	1.21
0.5	14.56	1.89	80.36	3.98
2.0	17.47	1.19	92.29	1.63
4.0	17.72	1.70	98.40	2.24

Table 4.3: Shape fixity and recovery stress of the braids with CNC content.

CNC wt% ratio	Shape fixity (%)		Recovery stress (MPa)	
	Mean	Standard deviation	Mean	Standard deviation
0.0	97.04	1.36	2.01	0.09
0.5	94.46	1.88	1.85	0.15
2.0	91.05	1.51	2.53	0.32
4.0	90.36	1.69	4.03	0.74

Chapter 5: Conclusions and future work

The aim of this study was to examine the capability of SMPU and CNC reinforced SMPU nanocomposites as an alternative braided suture material, which would have self-tightening feature due to SME. It was divided into two main parts. The first part investigated the effect of braiding parameters on overall mechanical and SME properties, while the second part did so for CNC reinforced SMPU nanocomposites. Former was conducted by producing 9 different type of braids with neat SMPU filaments based on two design parameters; number of core filaments and take-up speed of the braiding machine. In the latter, filaments and braids with different CNC wt% (0.5, 2.0, 4.0) were produced to test the effect of CNC wt% on mechanical and SME properties.

In the first part, mechanical tensile tests and shape recovery tests were conducted to examine the material's performance in glass and rubbery states, respectively, for both the braids and single filaments. Tensile tests revealed longitudinal elastic moduli and UTS. Due to the limitations of the stroke of the tensile test machine, samples were elongated to 90% strain, however, this amount was not enough for failure. Elastic modulus of the single filament was higher compared to braids, as expected. Take-up speed which is one of the key parameters in determination of the braid angle was proportional with the elastic modulus when the braids with same number of core filaments were compared. Furthermore, prediction model from previous literature was used with two different Poisson's ratio values to calculate elastic modulus analytically, and relatively accurate predictions were obtained when Poisson's ratio was set to 5. Elastic modulus of the braids and commercially available sutures were

compared, and it was concluded that they had similar levels of elastic modulus, while it is still possible to tailor elastic modulus through braiding parameters. The overall behavior of UTS values among different braids was similar to that of elastic moduli. UTS decreased with increasing braid angle. The contribution of the axial filaments to UTS, however, was more notable compared to elastic moduli. Braids with more core filaments had comparable UTS with the braids with fewer core filaments even though their braid angles were greater. Comparison of braided SMPU and commercially available sutures revealed that sutures are capable of withstanding higher tensile stresses -by an order higher in some cases- which revealed the insufficiency of braided SMPU in terms of strength. Shape recovery characteristics of the braids and single filament were also investigated since one of the main features was self-tightening ability for this potential SMP suture. Number of core filaments affected the recovery speed of the braids significantly, whereas take-up speed did not, which suggested that braid angle did not change the recovery rates. Maximum recovered strain was approximately 85% for all types of braids and single filament unlike the higher maximum recoveries reported in previous literature [49]. It is possible that this behavior was due to weight attachments which was normalized according to number of filaments. Recovery forces were larger for the braids with more core filaments, as expected. Recovery stresses were very close, with the single filament having the highest value even though there was a slight decrease in the case of three core filaments.

In the second part of this study, effects of CNC reinforcement were investigated by producing braided SMPU-CNC nanocomposites with 0.5, 2.0, 4.0 wt% CNC. Mechanical properties in glass state such as elastic modulus and UTS decreased by 11.7% and 22.2%, respectively,

with the addition of CNC, although the amount of CNC did not significantly affect the magnitude of this decline. It was discussed that the decline in mechanical properties was due to poor dispersion in line with the previous literature on nanocomposites with polymer matrix. In contrast, SME tests revealed much better results for CNC reinforced SMPU braids. Shape recovery rate, maximum shape recovery, recovery and programming stresses all showed substantial increase for 2.0 and 4.0 wt% CNC, especially for the latter. The feature where CNC reinforcement showed the most promise was the maximum recovery stress such that braids with 4.0 wt% CNC doubled the recovery stress of pure SMPU braids. The effect of CNC reinforcement was attributed to the high elastic modulus of CNC and the elastic deformation it stored when temporary shapes were set for the braids. For the same reason, shape fixity declined with increasing CNC wt%.

Following points express ways of extending the research work conducted in this thesis:

- Both pure SMPU and CNC reinforced SMPU lacked necessary tensile strength that commercially available sutures have. In future investigations, scanning electron microscope can be used to investigate dispersion characteristics, and better dispersion for CNC-SMPU nanocomposites can be aimed in order to increase tensile strength of the braided structure.

- SMPU MM4520, although biocompatible, is not biodegradable meaning that a possible suture would be nonabsorbable. Future studies may consider a biodegradable SMPU in order to produce an absorbable suture material.

- Mechanical properties of polymers depend heavily on strain rate. Therefore, shape recovery properties such as shape recovery rate and stress may be examined based on

different strain rates during the programming stage.

- Dynamic mechanical analysis can be conducted to determine viscoelastic properties such as storage and loss modulus.
- A possible SMP suture would be applied to tissue after setting the temporary shape. Hence, properties such as elastic modulus and tensile strength may be investigated after at least one shape recovery.

Bibliography

[1] Horeman, T., Meijer, E. J., Harlaar, J. J., Lange, J. F., Van Den Dobbelsteen, J. J., & Dankelman, J. (2013). Force sensing in surgical sutures. *PLoS ONE, 8*(12), 1-12.

[2] Lendlein, A. (2002). Biodegradable, elastic shape-memory polymers for potential biomedical applications. *Science, 296*(5573), 1673-1676.

[3] Rawal, A., Kumar, R., & Saraswat, H. (2012). Tensile mechanics of braided sutures. *Textile Research Journal, 82*(16), 1703-1710.

[4] Chu, C. C. (1981). Mechanical properties of suture materials: An important characterization. *Annals of Surgery, 193*(3), 365-371.

[5] Loutzenheiser, T. D., Harryman, D. T., Ziegler, D. W., & Yung, S. (1998). Optimizing arthroscopic knots using braided or monofilament suture. *Arthroscopy, 14*(1), 57-65.

[6] Kudur, M., Pai, S., Sripathi, H., & Prabhu, S. (2009). Sutures and suturing techniques in skin closure. *Indian Journal of Dermatology, Venereology and Leprology, 75*(4), 425-434.

[7] Tajirian, A. L., & Goldberg, D. J. (2010). A review of sutures and other skin closure materials. *Journal of Cosmetic and Laser Therapy, 12*(6), 296-302.

[8] Huang, W. M., Yang, B., Liu, N., & Phee, S. J. (2007). Water-responsive programmable shape memory polymer devices. In *International conference on smart materials and nanotechnology in engineering, 6423* (pp. 64231S). International Society for Optics and Photonics.

[9] Huang, W. M., Yang, B., & Fu, Y. Q. (2011). *Polyurethane shape memory polymers*. Florida: CRC Press.

[10] Auad, M. L., Contos, V. S., Nutt, S., Aranguren, M. I., & Marcovich, N. E. (2008). Characterization of nanocellulosereinforced shape memory polyurethanes. *Polymer International, 57*(4), 651-659.

[11] Small, W., Singhal, P., Wilson, T. S., & Maitland, D. J. (2010). Biomedical applications of thermally activated shape memory polymers. *Journal of Materials Chemistry, 20*(17), 3356-3366.

[12] Huang, W. M., Ding, Z., Wang, C. C., Wei, J., Zhao, Y., & Purnawali, H. (2010). Shape memory materials. *Materials Today, 13*(7-8), 54-61.

[13] Maitland, D. J., Metzger, M. F., Schumann, D., Lee, A., & Wilson, T. S. (2002). Photothermal properties of shape memory polymer microactuators for treating stroke. *Lasers in Surgery and Medicine, 30*(1), 1-11.

[14] Kim, J. H., Kang, T. J., & Yu, W. R. (2008). Mechanical modeling of self-expandable stent fabricated using braiding technology. *Journal of Biomechanics, 41*(15), 3202-3212.

[15] Ajili, S. H., Ebrahimi, N. G., & Soleimani, M. (2009). Polyurethane/polycaprolactane blend with shape memory effect as a proposed material for cardiovascular implants. *Acta Biomaterialia, 5*(5), 1519-1530.

[16] Baer, G. M., Small, W., Wilson, T. S., Benett, W. J., Matthews, D. L., Hartman, J., & Maitland, D. J. (2007). Fabrication and in vitro deployment of a laser-activated shape

memory polymer vascular stent. *Biomedical Engineering Online, 6*(1), 43. Retrieved from doi:10.1186/1475-925x-6-43.

[17] Yakacki, C. M., Shandas, R., Lanning, C., Rech, B., Eckstein, A., & Gall, K. (2007). Unconstrained recovery characterization of shape-memory polymer networks for cardiovascular applications. *Biomaterials, 28*(14), 2255-2263.

[18] Gall, K., Yakacki, C. M., Liu, Y., Shandas, R., Willett, N., & Anseth, K. S. (2005). Thermomechanics of the shape memory effect in polymers for biomedical applications. *Journal of Biomedical Materials Research Part A, 73*(3), 339-348.

[19] Wache, H. M., Tartakowska, D. J., Hentrich, A., & Wagner, M. H. (2003). Development of a polymer stent with shape memory effect as a drug delivery system. *Journal of Materials Science: Materials in Medicine, 14*(2), 109-112.

[20] Yakacki, C. M., Shandas, R., Safranski, D., Ortega, A. M., Sassaman, K., & Gall, K. (2008). Strong, tailored, biocompatible shapememory polymer networks. *Advanced Functional Materials, 18*(16), 2428-2435.

[21] Nakasima, A., Hu, J. R., Ichinose, M., & Shimada, H. (1991). Potential application of shape memory plastic as elastic material in clinical orthodontics. *The European Journal of Orthodontics, 13*(3), 179-186.

[22] Carey, J. P. (2016). Introduction to braided composites. In J. P. Carey (Ed.), *Handbook of advances in braided composite materials: Theory, production, testing and applications* (pp. 1-21). Woodhead Publishing.

[23] Kyosev, Y. (2014). *Braiding technology for textiles: Principles, design and processes.* Woodhead Publishing.

[24] Branscomb, D., Beale, D., & Broughton, R. (2013). New directions in braiding. *Journal of Engineered Fabrics & Fibers (JEFF), 8*(2), 11-24.

[25] Thakur, V. K., Thakur, M. K., & Gupta, R. K. (2013). Development of functionalized cellulosic biopolymers by graft copolymerization. *International Journal of Biological Macromolecules, 62*, 44-51.

[26] Fu, S., & Tian, C. (2015). Nanocellulose and its application for shape-memory materials. In V. K. Thakur, & M. K. Thakur (Eds.), *Eco-friendly polymer nanocomposites* (pp. 101-135). New Delhi: Springer.

[27] Marcovich, N. E., Auad, M. L., Bellesi, N. E., Nutt, S. R., & Aranguren, M. I. (2006). Cellulose micro/nanocrystals reinforced polyurethane. *Journal of Materials Research, 21*(4), 870-881.

[28] Cao, X., Habibi, Y., & Lucia, L. A. (2009). One-pot polymerization, surface grafting, and processing of waterborne polyurethane-cellulose nanocrystal nanocomposites. *Journal of Materials Chemistry, 19*(38), 7137-7145.

[29] Morin, A., & Dufresne, A. (2002). Nanocomposites of chitin whiskers from Riftia tubes and poly(caprolactone). *Macromolecules, 35*(6), 2190-2199.

[30] Pieczyska, E. A., & Tobushi, H. (2017). Thermomechanical coupling and localization effects examined in shape memory alloys and polymers by fast and sensitive infrared

camera. In Q. Sun, R. Matsui, K. Takeda, & E. A. Pieczyska (Eds.), *Advances in shape memory materials* (pp. 173-189). Cham: Springer.

[31] Villacres, J. F. (2017). *Additive manufacturing of shape memory polymers: Effects of print orientation and infill percentage on mechanical and shape memory recovery properties* (Unpublished master's thesis). University of Alberta.

[32] Garces, I., Aslanzadeh S., Boluk Y., & Ayranci, C. (in press). Effect of moisture on shape memory polyurethane polymers for extrusion based additive manufacturing - 4D Printing. *Additive Manufacturing*. Manuscript submitted for publication.

[33] Baer, G., Wilson, T. S., Matthews, D. L., & Maitland, D. J. (2007). Shape-memory behavior of thermally stimulated polyurethane for medical applications. *Journal of Applied Polymer Science, 103*(6), 3882-3892.

[34] Gordon, R. F. (1993). The properties and applications of shape memory polyurethanes. *Materials Technology, 8*(11-12), 254-258.

[35] Lin, N., & Dufresne, A. (2014). Nanocellulose in biomedicine: Current status and future prospect. *European Polymer Journal, 59*, 302-325.

[36] Garces, I., Aslanzadeh, S., Boluk, Y. & Ayranci, C. (in press). Cellulose nanocrystals (CNC) reinforced shape-memory polyurethane ribbons for future biomedical applications and design. *Journal of Thermoplastic Composite Materials*. Manuscript submitted for publication.

[37] ASTM D3822/D3822M-14. (2014). Standard test method for tensile properties of single textile fibers.

[38] Croarkin, C., Tobias, P., Filliben, J. J., Hembree, B., & Guthrie, W. (2006). *NIST/SEMATECH e-handbook of statistical methods*. NIST/SEMATECH. Retrieved from http://www.itl.nist.gov/div898/handbook.

[39] Prewitt, J. M. (1970). Object enhancement and extraction. *Picture Processing and Psychopictorics, 10*(1), 15-19.

[40] Satteson, E. S., & Molnar, J. A. (2017). Materials for wound closure. *Medscape*. Retrieved from https://emedicine.medscape.com/article/1127693-overview.

[41] Naleway, S. E., Lear, W., Kruzic, J. J., & Maughan, C. B. (2015). Mechanical properties of suture materials in general and cutaneous surgery. *Journal of Biomedical Materials Research - Part B Applied Biomaterials, 103*(4), 735-742.

[42] Omeroglu, S. (2006). The effect of braiding parameters on the mechanical properties of braided ropes. *Fibres and Textiles in Eastern Europe, 14*(4), 53-57.

[43] Rawal, A., Sibal, A., Saraswat, H., & Khan, S. Q. (2016). Topologically controlled tensile behaviour of braided prostheses for anterior cruciate ligaments. *Journal of the Mechanical Behavior of Biomedical Materials, 57*, 359-364.

[44] Dabiryan, H., Johari, M. S., Bakhtiyari, S., & Eskandari, E. (2017). Analysis of the tensile behavior of tubular braids using energy method, Part II: experimental study. *The Journal of the Textile Institute, 108*(11), 1899-1904.

[45] Kreszinger, M., Toholj, B., Aanski, A., Balo, S., Cincovi, M., Pein, M., Lipar M., & Smolec, O. (2018). Tensile strength retention of resorptive suture materials applied in the stomach wall - an in vitro study. *Veterinarski Arhiv, 88*(2), 235-243.

[46] Head, A. A., Ko, F. K., & Pastore, C. M. (1989). *Handbook of industrial braiding.* Covington, Kentucky: Atkins and Pearce.

[47] Hristov, K., Armstrong-Carroll, E., Dunn, M., Pastore, C., & Gowayed, Y. (2004). Mechanical behavior of circular hybrid braids under tensile loads. *Textile Research Journal, 74*(1), 20-26.

[48] Millett, P. J., Miller, B. S., Close, M., Sterett, W. I., Walsh, W., & Hawkins, R. J. (2003). Effects of braiding on tensile properties of four-strand human hamstring tendon grafts. *The American Journal of Sports Medicine, 31*(5), 714-717.

[49] Yang, B. (2007). *Influence of moisture in polyurethane shape memory polymers and their electrically conductive composites* (Unpublished doctoral dissertation). Nanyang Technological University.

[50] Auad, M. L., Mosiewicki, M. A., Richardson, T., Aranguren, M. I., & Marcovich, N. E. (2010). Nanocomposites made from cellulose nanocrystals and tailored segmented polyurethanes. *Journal of Applied Polymer Science, 115*(2), 1215-1225.

[51] Gall, K., Dunn, M. L., Liu, Y., Stefanic, G., & Balzar, D. (2004). Internal stress storage in shape memory polymer nanocomposites. *Applied Physics Letters, 85*(2), 290-292.

[52] Xie, X. L., Mai, Y. W., & Zhou, X. P. (2005). Dispersion and alignment of carbon nanotubes in polymer matrix: A review. *Materials Science and Engineering R: Reports, 49*(4), 89-112.

[53] Zhu, J., Kim, J. D., Peng, H., Margrave, J. L., Khabashesku, V. N., & Barrera, E. V. (2003). Improving the dispersion and integration of single-walled carbon nanotubes in

epoxy composites through functionalization. *Nano Letters, 3*(8), 1107-1113.

[54] Song, Y. S., & Youn, J. R. (2005). Influence of dispersion states of carbon nanotubes on physical properties of epoxy nanocomposites. *Carbon, 43*(7), 1378-1385.

Appendix A: Braid geometries

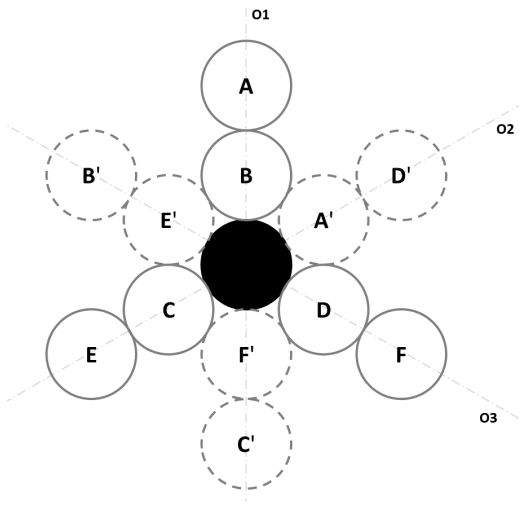

Figure A.1: Geometry of the braids with one core filament.

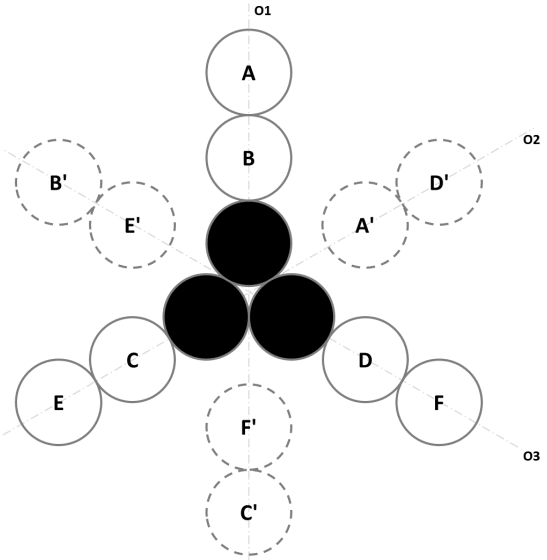

Figure A.2: Geometry of the braids with three core filaments.

Appendix B: Matlab script for optical strain measurement

```
clc; clear; close all;

%%
show_process = true;


%% CNC percentages
percentages = [0.5];


%% Struct array to put results in
Results = struct('Ratio',{});


for percentage = percentages

    %% Get test folders for this CNC percentage
    folders = dir(fullfile('images', num2str(percentage)));

    noffolders = length(folders) - 2;

    %% Analyze each folder
    for i = 5 : noffolders

        folderpath = fullfile('images', num2str(percentage), num2str(i));

        images = dir(folderpath); % Get names of the images
        images = images(~ismember({images.name}, {'.','..'}));

        braid_boundary = [];

        for j = 1 : length(images)

            % Read the image
            img = imread(fullfile(folderpath, images(j).name));

            img = img(:,1:1600);

            %% Find edges
            img = edge(img, 'Prewitt');

            %% Make braids white
            for k = 1 : length(img)

                whites = find(img(:,k));

                if length(whites) > 1
```

```
                upper = whites(1);
                lower = whites(end);

                img(upper:lower, k) = 1;

            end

        end


        if length(braid_boundary) > 1

            if braid_boundary(end) - braid_boundary(end-1) > 100

                braid_boundary(end) = braid_boundary(end-1);

            end

            start = max(1, braid_boundary(end) - 50);
            finish = start + 300;

        else

            start = 1;
            finish = 1500;

        end

        cols = sum(img(:,start:finish));

        indices = find(cols > 500);
        indices = fliplr(indices);

        for index = indices

            if ismember(index+1, indices) && ismember(index+2, indices)

                boundary = index;
                break;

            end

        end

        boundary = boundary + start - 1;

        if show_process

            imshow(img, 'InitialMagnification', 100);
            hold on;
            plot(start:finish, cols);
            tmp(1:660) = boundary;
            plot(tmp, 1:660, 'LineWidth', 2, 'Color', 'red');
            pause(0.1);
```

```
                hold off;

            end

            braid_boundary(end+1) = boundary;


            %% Display the progress
            clc;
            completed_perc = ceil( j / length(images) * 100);
            fprintf(['     CNC %%:\t%3.1f \n   Test no:\t%d \n ' ...
                'Completed:\t%d%%'], percentage, i, completed_perc);

        end

        index = length(Results) + 1;
        Results(index).Ratio = percentage;
        Results(index).BraidBoundaries = braid_boundary;

    end

end

clc;
clearvars -except Results;
```